



# Improving nitrogen cycling in a land surface model (CLM5) to quantify soil N<sub>2</sub>O, NO and NH<sub>3</sub> emissions from enhanced rock weathering with croplands

Maria Val Martin<sup>1</sup>, Elena Blanc-Betes<sup>2,3</sup>, Ka Ming Fung<sup>4</sup>, Euripides P. Kantzas<sup>1</sup>, Ilsa B. Kantola<sup>2,3</sup>,  
5 Isabella Chiaravalloti<sup>5</sup>, Lyla T. Taylor<sup>1</sup>, Louisa K. Emmons<sup>6</sup>, William R. Wieder<sup>6,7</sup>, Noah J. Planavsky<sup>5</sup>,  
Michael D. Masters<sup>2,3</sup>, Evan H. DeLucia<sup>2,3,8</sup>, Amos P.K. Tai<sup>4,9</sup> and David J. Beerling<sup>1</sup>

<sup>1</sup>Leverhulme Centre for Climate Change Mitigation, School of Biosciences, University of Sheffield, Sheffield, UK

<sup>2</sup>Institute for Sustainability, Energy, and Environment, University of Illinois at Urbana-Champaign, Urbana, IL, USA

<sup>3</sup>Carl R. Woese Institute for Genomic Biology, University of Illinois at Urbana-Champaign, Urbana, IL, USA

10 <sup>4</sup>Earth and Environmental Sciences Programme, Faculty of Science, The Chinese University of Hong Kong, Sha Tin, Hong Kong

<sup>5</sup>Department of Earth and Planetary Sciences, Yale University, New Haven, CT, USA

<sup>6</sup>National Center for Atmospheric Research, Boulder, CO, USA

<sup>7</sup>Institute of Arctic and Alpine Research, University of Colorado Boulder, Boulder CO, USA

15 <sup>8</sup>Department of Plant Biology, University of Illinois at Urbana-Champaign, Urbana, IL, USA

<sup>9</sup>State Key Laboratory of Agrobiotechnology and Institute of Environment, Energy and Sustainability, The Chinese University of Hong Kong, Sha Tin, Hong Kong

*Correspondence to:* Maria Val Martin (m.valmartin@sheffield.ac.uk)

20 **Abstract.** Surficial enhanced rock weathering (ERW) is a land-based carbon dioxide removal (CDR) strategy that involves applying crushed silicate rock (e.g., basalt) to agricultural soils. However, unintended biogeochemical interactions with the nitrogen cycle may arise through ERW increasing soil pH as basalt grains undergo dissolution that may reinforce, counteract, or even offset the climate benefits from carbon sequestration. Increases in soil pH could drive changes in the soil emissions of key non-CO<sub>2</sub> greenhouse gases, e.g., nitrous oxide (N<sub>2</sub>O), and trace gases, e.g., nitric oxide (NO) and ammonia (NH<sub>3</sub>) that  
25 affect air quality, and crop and human health. We present the development and implementation of a new improved nitrogen cycling scheme for the land surface model Community Land Model v5 (CLM5), the land component of the Community Earth System Model, allowing evaluation of ERW effects on soil gas emissions. We base the new parameterizations on datasets derived from soil pH responses of N<sub>2</sub>O, NO and NH<sub>3</sub> of ERW field trial and mesocosm experiments with crushed basalt. We successfully validated simulated ‘control’ (i.e., no ERW) seasonal cycles of soil N<sub>2</sub>O, NO and NH<sub>3</sub> emissions against a wide  
30 range of global emission inventories. We benchmark simulated mitigation of soil N<sub>2</sub>O fluxes in response to ERW against a sub-set of data from ERW field trials in the U.S. Corn Belt. Using the new scheme, we provide a specific example of the effect of large-scale ERW deployment with croplands on soil nitrogen fluxes across five key regions with high potential for CDR with ERW (North America, Brazil, Europe, India, and China). Across these regions, ERW implementation led to marked reductions in N<sub>2</sub>O and NO (both 18%) with moderate increases in NH<sub>3</sub> (2%). Our improved N-cycle scheme within CLM5 has  
35 utility for investigating the potential of ERW point-source and regional effects of soil N<sub>2</sub>O, NO and NH<sub>3</sub> fluxes in response to



current and future climates. This framework also provides the basis for assessing the implications of ERW for air quality given the role of NO in tropospheric ozone formation, and both NO and NH<sub>3</sub> in inorganic aerosol formation.

## 1 Introduction

Drastic and rapid emission reductions and the use of carbon dioxide (CO<sub>2</sub>) removal (CDR) technologies are essential for meeting the Paris Agreement on Climate and net-zero commitments (IPCC, 2021). Modelled scenarios indicate that 10-12 gigatons (Gt) of CO<sub>2</sub> must be removed and safely stored each year to limit warming to 2°C (Fuss et al., 2014). A series of land-based CDR strategies involving the terrestrial biosphere have been proposed, which includes afforestation and reforestation, bioenergy crops, enhanced rock weathering (ERW) and peatland restoration, among others. An overview of these land-based CDR strategies and recommendations for their application have been summarized by independent international expert committees (e.g., National Research Council, 2015, Royal Society, 2018) as well as the IPCC 2021 report (Canadell et al., 2021). All these reports agree that there are unidentified environmental risks that must be assessed, because they may reinforce, counteract, or even offset the climate benefits from carbon sequestration.

Land-based enhanced rock weathering is a CDR strategy, which involves applying crushed silicate rock (e.g., basalt) to soils to sequester carbon, and is potentially feasible for large-scale deployment with managed croplands and grazing lands. Basalt is an ideal abundant silicate rock for ERW because of its potential co-benefits for crop yields and capacity to reverse soil acidification (Kantola et al., 2017; Beerling et al., 2018). The estimated global net CDR potential for ERW deployed on main crop regions worldwide is 0.5–2 Gt CO<sub>2</sub> yr<sup>-1</sup> with extraction costs of US\$80–180 per tonne of CO<sub>2</sub> and carbon storage time scales of ≥10,000 years (Beerling et al., 2020). However, interactions between ERW, nitrogen (N) cycling, and soil-plant processes lead to changes in the emissions of other greenhouse gases (GHGs), e.g., nitrous oxide (N<sub>2</sub>O), methane (CH<sub>4</sub>), and atmospheric pollutants, e.g., nitrogen oxides (NO<sub>x</sub>=NO+NO<sub>2</sub>) and ammonia (NH<sub>3</sub>) from soils.

N<sub>2</sub>O is an important greenhouse gas and a long-lived stratospheric ozone-depleting substance (Prather et al., 2015). The concentration of atmospheric N<sub>2</sub>O has increased by more than 20% during the last centuries and is currently increasing at a rate of 2% per decade (Tian et al., 2020). Agricultural ecosystems are the largest anthropogenic source of N<sub>2</sub>O, with about 50% of the global emissions (Tian et al., 2020). Agricultural ecosystems are also significant sources of NH<sub>3</sub> and NO<sub>x</sub>, comprising about 80% of global NH<sub>3</sub> emissions (Van Damme et al., 2021) and about 10% of global NO<sub>x</sub> emissions (IPCC, 2021). Once emitted from soil, NH<sub>3</sub> and NO<sub>x</sub> species can lead to air pollution, by increasing N deposition as well as production of other air pollutants, such as ozone (O<sub>3</sub>) and particulate matter (PM, as PM<sub>2.5</sub> with particles with an aerodynamic diameter <2.5 μm and PM<sub>10</sub> with diameter <10 μm), which are harmful to human, ecosystem, and crop health. These nitrogen trace gases can also contribute to water eutrophication, soil acidification and loss of plant species and habitat diversity (e.g., Sutton et al., 2009). In the coming decades, soil nitrogen emissions in croplands are expected to continue to increase because of



fertilizer and manure application to meet the growing demand for food, forage, fibre, and energy (e.g., Reay et al., 2012; Davidson and Kanter, 2014; IPCC, 2021).

In agriculture ecosystems, soil  $\text{N}_2\text{O}$  and  $\text{NO}$  fluxes are driven by two main biochemical processes: nitrification and denitrification, while soil  $\text{NH}_3$  is driven by volatilization. These three processes are controlled by many environmental factors such as temperature, soil pH, water and oxygen content and N availability (via synthetic fertilizer and manure applications) (e.g., Reay et al., 2012; Tian et al., 2016). Analyses from enhanced weathering field experiments in the U.S. Corn Belt have shown that the application of basalt consistently increases soil pH and reduces soil  $\text{N}_2\text{O}$  fluxes with no effects on soil  $\text{CO}_2$  emissions (Blanc-Betes et al., 2020). It is expected that increases in soil pH will concurrently produce a decrease in soil  $\text{NO}_x$  emissions, by decreasing rates of denitrification and nitrification (Parson et al., 2001) and an increase in  $\text{NH}_3$  volatilization (Mkhabela et al., 2006). Thus, widespread implementation of ERW holds consequences for air quality and human and crop health as well as for climate mitigation that have so far been overlooked. To date, there is no modelling framework that has the capability to fully quantify the changes in biogeochemical processes and atmospheric trace gas emissions from ERW applications.

In this study, we present the development and implementation of a new improved N cycling scheme for the land surface model Community Land Model v5 (CLM5), the land component of the Community Earth System Model, allowing evaluation of ERW effects on soil nitrogen gas emissions. We base the new parameterizations on datasets derived from soil pH responses of  $\text{N}_2\text{O}$ ,  $\text{NO}$  and  $\text{NH}_3$  in ERW field trial and mesocosm experiments with crushed basalt. Finally, we present a case examining the impact of large-scale deployment of ERW on main croplands across the world on  $\text{N}_2\text{O}$ ,  $\text{NO}$  and  $\text{NH}_3$  emissions.

## 2 Methodology

### 2.1 The Community Land Model version 5 (CLM5)

We implemented new parameterizations into the Community Land Model version 5.0.25 (CLM5; Lawrence et al., 2019) to determine  $\text{N}_2\text{O}$  and  $\text{NO}$  fluxes, and  $\text{NH}_3$  volatilized from soil due to basalt amendments in crops. CLM is the terrestrial component of the Community Earth System Model version 2 (CESM2; Danabasoglu et al., 2020). CLM5 represents terrestrial carbon and nitrogen cycling with prognostic vegetation and crop growth. The model uses a sub-grid hierarchy in which grid cells are composed of multiple land units, columns, and patches to represent the spatial land surface heterogeneity and the biogeophysical and biogeochemical differences between various land types within a model grid cell. The CLM5 land units are vegetated, lake, urban, glacier, and crop. Vegetation and crops are represented by plant and crop functional types (PFTs and CFTs), each with its own set of ecophysiological, morphological, phenological, and biogeochemical parameters (Levis et al., 2018). The default PFT distribution of natural vegetation and crops are derived from satellite observations (e.g., MODIS) and agricultural census data (Lawrence and Chase, 2007; Portmann et al., 2010). There are 16 types of natural vegetation (including bare ground) and eight active crops (temperate soybean, tropical soybean, temperate corn, tropical corn, spring wheat, cotton,



rice, and sugarcane) (Lombardozi et al., 2020). In CLM5, natural vegetation and croplands are treated on separate columns and isolate particular management practices, i.e., natural vegetation is handled in single unmanaged soil columns sharing a single pool of water and nutrients, whereas each crop has a dedicated column (Drewniak et al., 2013).

100 For crops, CLM5 provides nutrients from the mineral N pool in the soil, which is supplied through organic matter decomposition, N deposition, N fixation and fertilization. The interactive N fertilization scheme in CLM5 simulates fertilization by adding N directly to the soil mineral  $\text{NH}_4^+$  pool to meet crop N demands using both synthetic fertilizer and manure application. Fertilizer is applied to each crop for 20 successive days uniformly as soon as the crops enter the leaf emergence phase and is added in each layer from ground surface to 0.4 m depth according to the model-defined soil profile  
105 (Lawrence et al., 2019). CLM5 simulates the beginning of plant growth stages (seedling, leaf emerging, and grain filling) as well as crop sowing dates and planting durations based on the cumulative warm-enough hours at the beginning of spring. Crops are harvested once they reach maturity or a predefined maximum growing days (typically 150–165 days) (Lawrence et al., 2019; Lombardozi et al., 2020).

## 2.2 Updates and implementations in the soil nitrogen scheme

110 Figure 1 summarizes the main processes of the terrestrial N cycle in CLM5, following the ‘holes-in-a-pipe’ concept (e.g., Firestone and Davidson, 1989; Davidson and Verchot, 2000; Inatomi et al., 2019), highlighting the main implementations in this work. The model tracks N content in soil, plants, and organic matter as a series of distinct N pools, with biogeochemical processes acting as N exchange fluxes across them. Soil N transformations occur in vertically resolved soil profiles in each soil column following a Century-like implementation of soil biogeochemistry (Koven et al., 2013; Lawrence et al., 2019).  
115 Plant uptake, microbial immobilization, N mineralization, nitrification, and denitrification compete for soil mineral nitrogen ( $\text{NH}_4^+$  and  $\text{NO}_3^-$ ) based on the relative demand from each process. The release of  $\text{N}_2\text{O}$  as byproduct of nitrification and denitrification, and the leaching of soil nitrate ( $\text{NO}_3^-$ ) result in N losses from terrestrial ecosystems, which are replaced through fertilization, atmospheric N deposition, and biological N fixation (both symbiotic and asymbiotic). In this study, we modify CLM5 to better simulate the terrestrial nitrogen cycle by implementing soil NO fluxes and  $\text{NH}_3$  from volatilization and  
120 integrating regulating functions of soil pH that allows to evaluate the potential impact of basalt amendments on soil nitrogen gas fluxes.

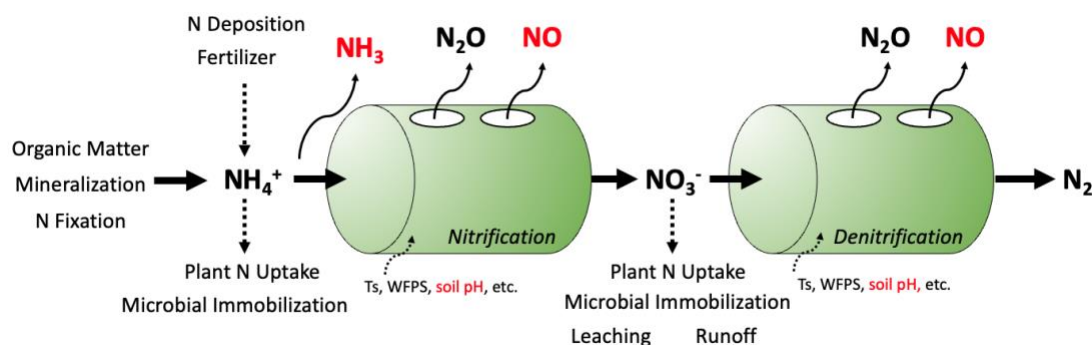


**Figure 1: Conceptual diagram of nitrogen cycle and the “holes-in-a-pipe” approach. Parameters in red are new additions in the default model. Ts is soil temperature; WFPS is water-filled pore space; and N is nitrogen.**

### 125 2.2.1 Inorganic N transformations, soil N<sub>2</sub>O fluxes and soil pH

Nitrification and denitrification processes in CLM5 are based on the process-based biogeochemical model DAYCENT (Parton et al., 1996; Del Grosso et al., 2000; Del Grosso et al., 2006). For nitrification fluxes, we included the dependency of N mineralization-based term on potential nitrification rates that was implemented in Parton et al. (2001), which was missing from previous versions of CLM5 (Nevison et al., 2022a). Under this scheme, 20% of mineralized nitrogen is nitrified.

130 CLM5 assumes a constant fraction to be N<sub>2</sub>O produced from nitrification ( $fN_{2O_{nit}} = 6 \times 10^{-4}$ ; Li et al., 2000). However, this N<sub>2</sub>O production depends on environmental conditions like soil temperature, water content and pH (Inatomi et al., 2020 and references therein). Considering an independent N<sub>2</sub>O emission fraction linked to environmental conditions provide better estimates of N<sub>2</sub>O emissions. To incorporate the effect of basalt addition on nitrification N<sub>2</sub>O fluxes via regulating soil pH, we adopted a modified pH-based function ( $fN_{2O_{nit}}$ ) proposed by Inatomi et al., (2020) based on a meta-analysis:

135 
$$fN_{2O_{nit}} = 721.86 \times e^{-2.387 \times \text{pH}}$$

The updated  $fN_{2O_{nit}}$  function made the nitrification rate in CLM5 go from the global constant average of 0.06% to 0.3% and increased the global N<sub>2</sub>O nitrification/denitrification ratio from 1% to 14%, more accordingly to previous estimates (Inatomi et al., 2020). As CLM5 uses a fixed pH value of 6.5 across all soils (Lawrence et al., 2019), we implemented the global soil pH from the Harmonized World Soil Database (FAO, 2012; Wieder et al., 2014). This dataset provides global spatial  
 140 distribution of soil pH and other soil properties for surface (0 to 30cm) and deeper soils (30 to 100 cm) at 0.05-degree spatial resolution, and regridded to the CLM5 resolution (0.9x1.25) for the nominal year of 2000 (Fig. S1 in Supplementary Material (SM)). We further distributed the topsoil and subsoil soil pH values through the CLM5 soil layers accordingly.

Denitrification also produces N<sub>2</sub>O as a byproduct (Fig. 1). To model the effect of basalt addition on N<sub>2</sub>O fluxes from denitrification, we included the updated denitrification scheme of Blanc-Betes et al., (2020). As in CLM5, Blanc-Betes et al.,



145 (2020)'s scheme is a modified version of the DAYCENT denitrification subroutine (Parton et al., 1996; Del Grosso et al., 2000) with the difference that it incorporates the effects of soil pH on gross denitrification rates ( $N_2 + N_2O$ ) and on the stoichiometry of denitrification end products ( $R_{N_2:N_2O}$  ratio).

For the total N loss during denitrification, the pH effect function ( $f_{pH}$ ) was based on Liu et al. (2010) and Rochester (2003):

$$f_{pH} = 0.0016e^{1.006 \times pH}$$

150 For the  $N_2$  to  $N_2O$  ratio of the end products, we included the pH effect function ( $f_{pH}$ ) adapted from Wagena et al. (2017) with adjusted thresholds:

$$f_{pH} = \begin{cases} 0.001 & \text{for } pH \leq 4 \\ 0.001 + \frac{pH - 4}{3} & \text{for } 4 < pH < 7 \\ 1.0 & \text{for } pH \geq 7 \end{cases}$$

More information about the scheme, model calibration and validation with basalt observations in crops is provided by Blanc-Betes et al (2020).

### 155 2.2.2 Soil NO fluxes

In addition to the modifications in the  $N_2O$  scheme, we implemented a new parameterization to calculate NO released as by-products of nitrification and denitrification. We used the ratio of NO to  $N_2O$  to account for the emission of NO during nitrification and denitrification based on Parton et al., (2001) and Zhao et al., (2017):

$$R_{NO:N_2O} = 15.2 + \frac{35.5 \tan^{-1}[0.75\pi(10D_r - 1.86)]}{\pi},$$

160 where  $D_r$  is the soil relative gas diffusivity in soil with respect to air and is calculated as a function of air-filled pore space (AFPS) of soil (Davidson and Trumbore, 1995):

$$D_r = 0.209AFPS^{\frac{4}{3}},$$

where AFPS is  $1 - \frac{\theta_v}{\theta_{v,sat}}$  and  $\theta_v$  and  $\theta_{v,sat}$  are instantaneous and saturated volumetric soil water content (in  $m^3 m^{-3}$ ), respectively.

165 NO emitted from soils is quickly oxidized to  $NO_2$  by  $O_3$  near the canopy, and the formed  $NO_2$  may be deposited onto the plant canopy (Bakwin et al., 1990; Jacob and Wofsy, 1990). To account for the loss of NO to plant canopy, we applied a canopy reduction scaling factor (CRF; Fig. S2 in SM) based on Yan et al (2005):

$$CRF = \frac{e^{-K_S \times SAI} + e^{-K_C \times LAI}}{2},$$



170 where SAI and LAI are stomatal area index and leaf area index, respectively, and  $k_s$  and  $k_c$  are 11.6 and 0.32, respectively. The corresponding SAI was derived from the SAI:LAI ratio of Yienger and Levy (1995). NO captured from the atmosphere is uptaken by the plant system either by direct incorporation into the leaf tissues or by the roots after absorption into the soil (Yoneyama et al., 1980). Since the precise mechanisms underlying these two routes is uncertain and fall outside the scope of this study, we assumed that all captured NO is returned to the soil directly as  $\text{NH}_4^+$ .

We also included a rain pulse factor to the base NO flux associated with nitrification to simulate the rapid increase of NO  
175 fluxes following rain onto a previous dry soil period (e.g., Parton et al., 2001; Yan et al., 2005; Hudman et al., 2012) as:

$$P_{peak} = 13.01 \ln(I_{dry}) - 53.6 \times e^{-ct},$$

where  $P_{peak}$  represents the magnitude of the peak flux relative to the pre-wetting flux and the value of  $I_{dry}$  is the antecedent dry period in hours. The  $c$  is a rate constant representing the rise/fall time of the pulse ( $0.068 \text{ h}^{-1}$ ) and  $t$  is time-step in hours.  $P_{peak}$  depends logarithmically on the length of the antecedent dry period and the condition for a pulse is a change in soil moisture.  
180 To test for pulsing potential, we employed the two-part condition as in Yan et al., (2005). Dry soil is defined as soils with a moisture content below 17.5% (v/v). To trigger a pulse, an increase of more than 0.5% (v/v) in the moisture content of soil that experiences dry conditions for at least 3 days is required. This increase of 0.5% (v/v) in 7 cm of surface soil is equivalent to about 3.5 mm of rainfall, which is the rainfall amount previously reported to cause a pulse (e.g., Johansson and Sanhueza, 1988; Martin et al., 1998).

185 Following Parton et al., (2001), total NO emissions from soils and released above canopy are thus calculated as a function of the simulated  $\text{N}_2\text{O}$  fluxes, the  $R_{\text{NO}:\text{N}_2\text{O}}$  function, the factor to account for rain pulses in NO emission initiated by precipitation events (P) and the CRF:

$$\text{Soil NO}_{\text{soil}} = \text{N}_2\text{O}_{\text{denit}} \times R_{\text{NO}:\text{N}_2\text{O}} + \text{N}_2\text{O}_{\text{nit}} \times R_{\text{NO}:\text{N}_2\text{O}} \times P$$

$$\text{Soil NO}_{\text{above-canopy}} = \text{Soil NO}_{\text{soil}} \times \text{CRF}$$

### 190 2.2.3 Soil $\text{NH}_3$ volatilization

For  $\text{NH}_3$  volatilization, we used the scheme implemented by Fung et al., (2022) and embedded within the CLM5 N cycle. This scheme is derived from the DeNitrification-DeComposition (DNDC) biogeochemical model (Li et al., 2012) and includes a further parameterization to account for released  $\text{NH}_3$  that is captured in the plant canopy. As in the soil NO scheme, we assumed all captured  $\text{NH}_3$  returns to the soil directly as  $\text{NH}_4^+$ . In this scheme,  $\text{NH}_3$  is very sensitive to soil pH, as it grows exponentially  
195 with pH, in the order of  $10^{\text{pH}}$ . As shown by Fung et al., (2022), the use of a spatially distributed soil pH database is not feasible as it overestimates  $\text{NH}_3$  fluxes in alkaline soils ( $\text{pH} > 6.5$ ). This is a well-known limitation in current  $\text{NH}_3$  schemes (e.g., Sutton et al., 2013; Vira et al., 2020), where functions are not parameterized for global applications, and further work is needed for global models to accurately describe soil pH effects on  $\text{NH}_3$  fluxes. In this work, we kept the soil pH constant to 6.5 to estimate



a consistent NH<sub>3</sub> flux baseline and added a unit factor ( $f_{pH}$ ) as a function of soil pH to model the effect of basalt addition on  
200 NH<sub>3</sub> fluxes. The new regulating  $f_{pH}$  function is based on previous observations of NH<sub>3</sub> and soil pH from lime (Mkhabela et  
al., 2006), biochar (Kim et al., 2021) and basalt applications (Chiaravalloti, 2023) (Fig. S3 in SM):

$$f_{pH} = \begin{cases} 0.6 & \text{for pH} < 5 \\ 0.6 \times \frac{0.4}{3 \times (\text{pH} - 5)} & \text{for } 5 \leq \text{pH} \leq 8 \\ 1.0 & \text{for pH} > 8 \end{cases}$$

This function is a first approximation, which allows releasing some NH<sub>3</sub> in very acidic crop soils (pH < 5.5), whereas  
increasingly NH<sub>3</sub> volatilization losses occur in higher soil pH with a saturation at relatively high soil pH levels (>8).  
205 Observations on the magnitude of soil pH in controlling NH<sub>3</sub> volatilization fluxes from basalt applications are very scarce.  
However, our proposed changes in  $f_{pH}$  are fairly consistent with soil pH effects in NH<sub>3</sub> volatilization observed in field  
measurements in a marshland soil with lime application (Mkhabela et al., 2006), experimental measurements from basalt  
application (12.5 t rock ha<sup>-1</sup>) in a greenhouse setting (Chiaravalloti, 2023) and chamber experiments with 3% biochar and  
liquid fertilizers (Kim et al., 2021). Further observations of NH<sub>3</sub> volatilization rates from basalt application under wider range  
210 of soil pH conditions are urgently needed to verify the actual effect of soil pH.

### 2.3 CLM5 ERW simulations

We performed single-point simulations at the Energy Farm field site (University of Illinois, U.S.) to examine the model  
sensitivity to basalt applications in maize and soybean crops and soil and climate conditions. We spun-up the model for about  
800 years, so that all the state variables in the model, especially total ecosystem soil carbon reached equilibrium. The present-  
215 day spin-up was based on a historical simulation 1850–2014, using historical N and aerosol deposition, atmospheric CO<sub>2</sub>  
forcing and meteorological forcings from GSWP3 version (Lawrence et al., 2019), with soil texture and soil pH values based  
on onsite measurements in Control and ERW plots at the Energy Farm (Beerling et al., submitted). Following the historical  
simulation, the Energy Farm simulations were run from 2015 to 2019 with meteorological forcing data retrieved from the  
North American Land Data Assimilation System (NLDAS) forcing dataset (Xia et al., 2012), and initial conditions starting in  
220 2015 for the two single-point simulations, without basalt ('Control' Run) and with basalt ('ERW' Run) application.

In addition to single-point simulations, we performed global simulations to validate the new implementation at large scale and  
assess the regional effects of basalt treatments to soil direct agricultural N fluxes. We first spun-up CLM5 with the new  
implementations to steady state in 1850 using an accelerated decomposition procedure and fixed pre-industrial CO<sub>2</sub>, land use,  
and atmospheric N deposition (Lawrence et al., 2019). We initialized CLM5 simulations for 2000 using fully spun-up  
225 conditions. The present-day spin-up was based on a historical simulation 1850–2014, using historical N and aerosol deposition,  
atmospheric CO<sub>2</sub> forcing, and land use change (Lawrence et al., 2019). The meteorological forcings were from the Global Soil



Wetness Project (GSWP3 version 1; <http://hydro.iis.u-tokyo.ac.jp/GSWP3/>), with forcing data available from 1901 to 2014 and cycled from 1901 to 1920 for years prior to 1901.

To model the effect of basalt addition on the  $\text{N}_2\text{O}$ , NO and  $\text{NH}_3$  fluxes from soil, we developed a weathering module for CLM5, in which dynamic annual or monthly changes in soil pH estimated by an ERW model (Beerling et al., 2020; Kantzas et al., 2022) are read within the CLM5 N cycle. In this work, we considered the soil pH changes as well as application locations across five key regions with high potential for CDR with ERW (North America, Brazil, Europe, India, and China) required to remove 2Gt  $\text{CO}_2$  per year (Beerling et al., 2020). To test the new scheme at a global scale, we used changes in annual soil pH (Fig. 2 and Fig. S4 in SM); dynamic changes of soil pH in monthly timesteps were tested in a regional study for the UK (Kantzas et al., 2022).

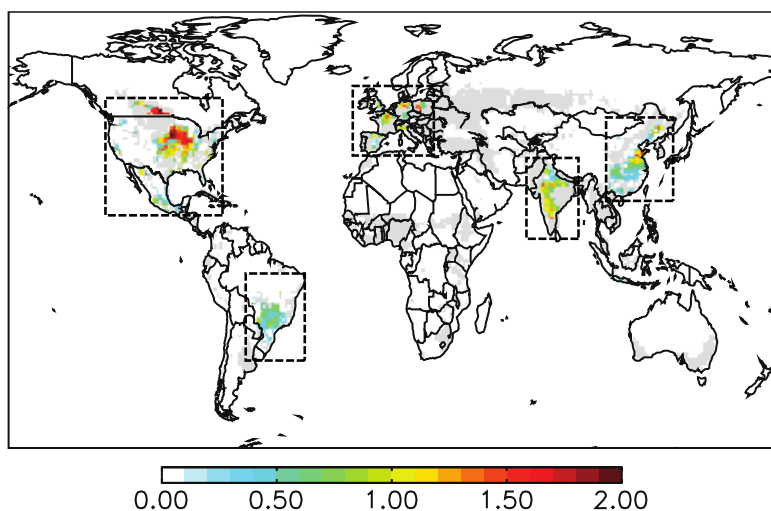


**Figure 2: Changes in soil pH after annual basalt applications in a 25-year timeframe to remove 2 Gt  $\text{CO}_2$  (Beerling et al., 2020). Delimited are the five agriculture regions considered in this study; shaded in grey are grid cells with crops (> 10%), in which basalt was not applied. A close-up view for each region is in Figure S4 in SM.**

Simulations were completed at a resolution of  $0.9^\circ$  latitude by  $1.25^\circ$  longitude and with a 30-min time step. We used the mean and standard deviation of the last 5 years (2010–2014) of the historical simulations as an approximation of present-day conditions of the modelled N cycle, for a Control Run (without basalt) and an ERW Run (with basalt). In both simulations, synthetic fertilizer application was prescribed by crop type on the Land Use Model Intercomparison Project (Hurtt et al., 2011) and manure fertilizer was applied at a fixed rate for all crops ( $20 \text{ kg N ha}^{-1} \text{ yr}^{-1}$ ; Lombardozzi et al., 2020).

## 2.6 Datasets for model validation

We used observational data collected at the University of Illinois Energy Farm in 2016–2019. The Energy Farm is in central Illinois ( $40.06^\circ \text{ N}$ ,  $88.19^\circ \text{ W}$ ) and the historic land use is corn-soy agriculture (Cheng et al., 2020; Blanc-Betes et al., 2020). In



the spring of 2016, a pilot ERW experimental study was conducted using twenty, 2 x 2 m plots in a field of maize; a field-scale experiment was initiated in 2017. This large-scale field experiment consists of several ERW experimental plots of 3.8  
250 ha (200x200 m) each in size, with control and basalt-treated plots, each instrumented with an eddy covariance system at the centre of the plot to measure surface energy, water, and carbon fluxes (Zeri et al., 2011). Soil pH is measured through surface soil samples (0–10 and 10–30 cm) and N<sub>2</sub>O fluxes were monitored through static chambers atop PVC collars during the planting season (Beerling et al., submitted).

We also compared our global simulation results with available observations and emission inventories. Simulated CLM5  
255 nitrogen emissions are compared with multiple emission inventories, including the Copernicus Atmosphere Monitoring Service (CAMS; Bennouna et al., 2020), Community Emissions Data System (CEDS; Hoesly et al., 2018), Emission Database for Global Atmospheric Research (EDGAR; Crippa et al., 2018) and Harmonized Emissions Component (HEMCO; Lin et al., 2021). For N<sub>2</sub>O, we also used results from the global N<sub>2</sub>O Model Intercomparison Project (NMIP; Tian et al., 2018), and estimates from Wang et al., (2020) and the CarbonTracker Lagrange North American Regional Inversion Framework (Nevison  
260 et al., 2018). Details of all these datasets are presented in Table 1. The datasets were regridded to match our model resolution of 0.9 by 1.25 using bilinear interpolation. It is important to note that our CLM5 model-inventory comparison should not be considered quantitative, but rather qualitative because our simulations do not match the meteorological years of the inventories and because actual manure and synthetic fertilizer usage in CLM5 may differ from what was assumed in the inventories.

265

270

275



**Table 1. Summary of observations and emission inventories used in this study for model comparison and validation.**

Name and Reference	Coverage	Resolution	Period	Notes
CAMS (Granier et al., 2018)	Global	0.1° x 0.1° Monthly	2010–2019	NO and NH <sub>3</sub> from agricultural soils and nitrogen deposition
CEDS (Hoesly et al., 2018)	Global	0.01° x 0.01° Monthly	2005–2015	NO and NH <sub>3</sub> from agricultural soils with both synthetic and manure fertilizers
EDGAR (Crippa et al., 2018)	Global	0.1° x 0.1° Monthly	2010	N <sub>2</sub> O, NO, NH <sub>3</sub> from agricultural soils with both synthetic and manure fertilizers
HEMCO (Lin et al., 2021)	Global	0.5° x 0.625° Monthly	2005–2017	NO soil emissions weighted by CLM5 gridded crop area
NMIP (Tian et al., 2018)	Global	0.5° x 0.5° Annual & Monthly	2000–2015	Modeled N <sub>2</sub> O fluxes in crops from the global N <sub>2</sub> O Model Intercomparison Project
Wang et al., (2020)	Global	0.1° x 0.1° Annual	2010–2014	Modeled N <sub>2</sub> O fluxes in crops with an empirical upscaling method using site-level observations spatially distributed
Nevison et al., (2018)	USA	1° x 1° Daily	2008–2015	N <sub>2</sub> O fluxes from an inversed model with atmospheric N <sub>2</sub> O observations

### 3 Validation

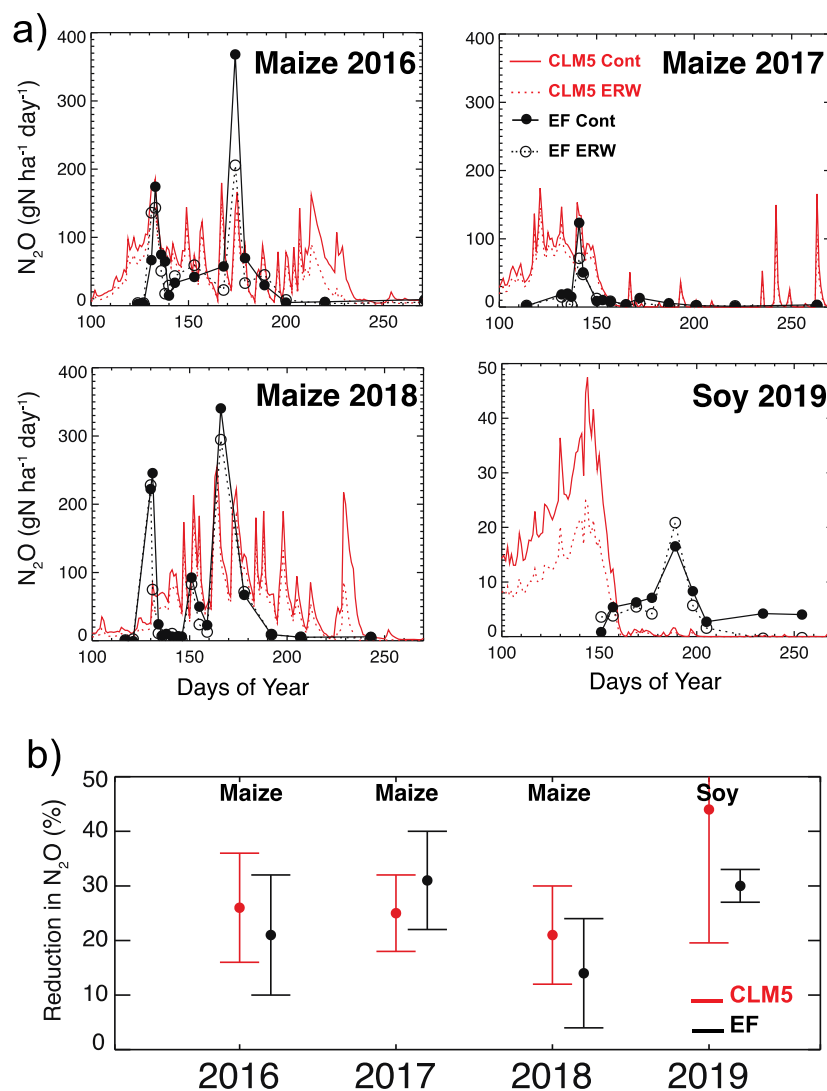
CLM5 simulations have been extensively evaluated by comparison with observations on a global scale (e.g., Lawrence et al., 2019; Lombardozzi et al., 2020; Nevison et al., 2022b) as well as in specific field sites (e.g., Chen et al., 2020, Nevison et al., 2022a). We focus our evaluation on soil N<sub>2</sub>O fluxes from croplands at the Energy Farm, continental U.S., and agriculture N<sub>2</sub>O, NO<sub>x</sub> and NH<sub>3</sub> emissions at a global scale and the response of the simulated soil N<sub>2</sub>O to changes in soil pH from basalt applications.



### 3.1 Soil N<sub>2</sub>O at the Energy Farm and continental U.S.

285 Figure 3 compares modeled soil N<sub>2</sub>O in our single-point simulations with available observations at the Energy Farm pre-trail  
(maize) in 2016 and trial rotation crops (maize, maize, and soybean) in 2017–2019. For daily soil N<sub>2</sub>O fluxes (Fig. 3a), we  
found that simulated daily N<sub>2</sub>O showed generally good agreement with the limited daily observations at the Energy Farm,  
simulating larger averaged soil N<sub>2</sub>O fluxes during the growing season in maize (37.2–51.7 gN ha<sup>-1</sup> day<sup>-1</sup>) than soybean (7.2  
290 gN ha<sup>-1</sup> day<sup>-1</sup>), similar to what was observed in the field trails (18.8–62.3 gN ha<sup>-1</sup> day<sup>-1</sup> for maize and 6.2 gN ha<sup>-1</sup> day<sup>-1</sup> for  
soybean). As shown for DAYCENT by Blanc-Betes et al., (2020), CLM5 also simulates well the increased in N<sub>2</sub>O fluxes  
following fertilization and precipitation events at the Energy Farm, although with daily fluxes peaking slightly earlier in the  
growing season compared to observations due to yearly differences in planting schedule and fertilization, and a  
misrepresentation of biological N fixation for soy crops. It is important to note that in this project CLM5 has not been calibrated  
specifically for the Energy Farm conditions or across the U.S., rather used as in the released version as the objective is to use  
295 the model at a global scale, across many crops and for future climate projections.

To determine if CLM5 simulates soil N<sub>2</sub>O changes due to basalt amendments, we compared the relative changes in N<sub>2</sub>O in the  
basalt-treated plots with respect the control plots for each year, at the Energy Farm and simulated by the model in Fig. 3b. The  
changes in N<sub>2</sub>O were obtained by comparing the cumulative N<sub>2</sub>O at the end of the growing season using the measured and  
simulated N<sub>2</sub>O flux at the time of the discrete measurements. For the basalt amendment run in CLM5, we considered the same  
300 increases in soil pH observed in the field experiments (section 2.3; Beerling et al., submitted). We found that CLM5 effectively  
reproduces the decrease in soil N<sub>2</sub>O in the basalt-treated plots with soil N<sub>2</sub>O fluxes 21–25% (maize) and 44% (soy) smaller  
than control plots, in line with the observed decreases of 12–32% and 31% at the Energy Farm.

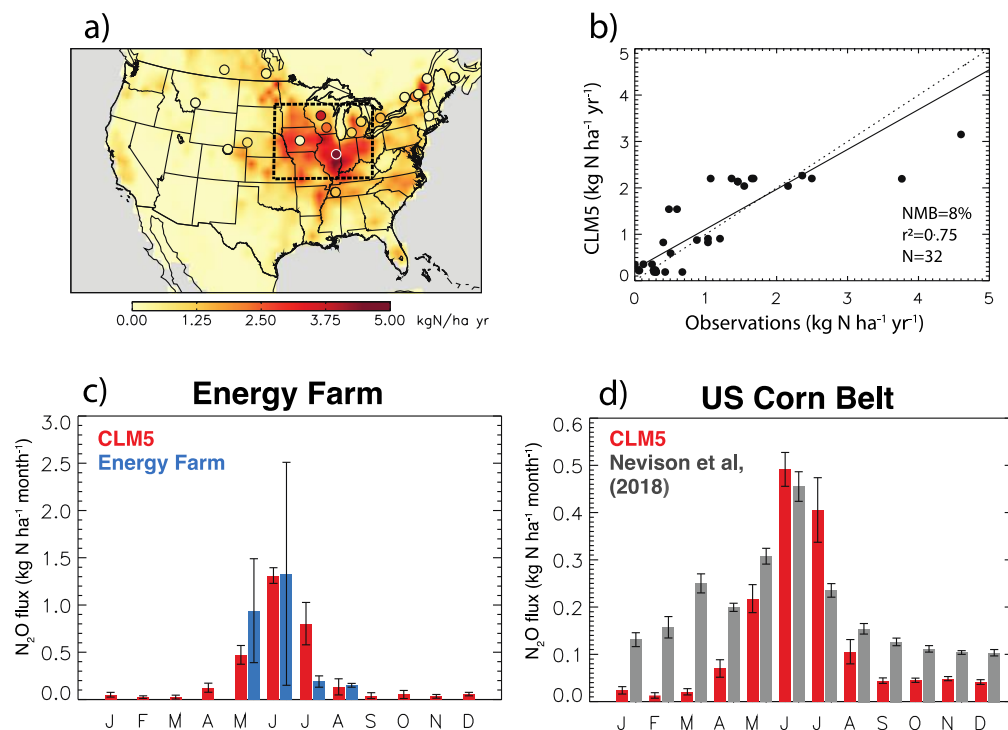


305 **Figure 3: Soil N<sub>2</sub>O fluxes at the Energy Farm for the pilot study (maize; 2016) and the large field trials (rotation crops as maize, maize and soybean; 2017–2019). Shown is simulated (red) and observed (black) daily N<sub>2</sub>O fluxes (g N ha<sup>-1</sup> day<sup>-1</sup>) at the control (solid lines or solid circles) and basalt-treated plots (dotted lines or open circles) (a) and reductions in N<sub>2</sub>O emissions (%) in the basalt-treated plots compared to the control plots for the simulated by CLM5 (red) and measured at the field experiments (black) (b).**

310 We used observations of N<sub>2</sub>O from agricultural fields summarized in published studies (e.g., Stehfest and Bouwman, 2006; Shcherbak et al., 2014; Wang et al., 2018), including the Energy Farm, and N<sub>2</sub>O emissions estimated across North America using the Carbon Tracker-Lagrange regional inversion framework (Nevison et al., 2018) to assess how well CLM5 captures



agriculture N<sub>2</sub>O emissions in the U.S., an important agricultural region suitable for large-scale ERW deployment (Beerling et al., 2020) (Fig. 4).



315

**Figure 4: Soil N<sub>2</sub>O fluxes in U.S. with modelled and observed values at individual measurement sites (a), the scatter plot with modelled and observed values at the individual sites (b), seasonal variability of monthly soil N<sub>2</sub>O at the location of the Energy Farm (c) and across the US Corn Belt (d). Observations are means from published measurements, including the Energy Farm (2017-2019; Blanc-Betes et al., 2021) or averaged monthly fluxes from the Carbon Tracker-Lagrange regional inversion model (2008-2014; Nevison et al., 2018). The squared-correlation coefficient ( $r^2$ ), nominal mean bias (NMB, %) and number of observations (N) are shown in the inset. Reduced major axis-regression lines (solid) for croplands and the 1:1 line (dashed) are also shown. The US Corn Belt is represented with a dashed box and location of Energy Farm (40.07 N, 88.2 W) with a white border circle in the CLM5 map. Error bars represent the standard deviation of the annual totals.**

325

For our studied period, CLM5 estimates a total N<sub>2</sub>O emission across continental U.S. croplands of  $0.59 \pm 0.06$  Tg N<sub>2</sub>O-N yr<sup>-1</sup>, with more than 50% emitted in the U.S. Corn Belt. Our soil N<sub>2</sub>O emissions fall well within the range of previous estimates for direct agriculture emissions in the U.S. (0.3–1.1 Tg N yr<sup>-1</sup>) reported by the U.S. Environmental Protection Agency (EPA), bottom-up inventories, and other processed-based land models (e.g., Tian et al., 2019; Lu et al., 2021; U.S. EPA, 2022). Similar to other studies, our modelled estimates are lower than those reported from top-down N<sub>2</sub>O studies (1.6–2.6 Tg N yr<sup>-1</sup>; Miller et al., 2012; Nevison et al., 2018) as they consider more N<sub>2</sub>O source types than direct agriculture emissions, e.g., fossil fuel

330



combustion, industry non-combustion processes, biomass burning, and solid waste and sewage water. For the U.S. Corn Belt, dominated by agriculture sources, our annual flux ( $0.31 \pm 0.04 \text{ Tg N}_2\text{O-N yr}^{-1}$ ) is comparable to that from top-down estimates ( $0.32\text{--}0.42 \text{ Tg N yr}^{-1}$ ; Griffins et al., 2013; Chen et al., 2016; Nevison et al., 2018) as well as previous estimates with process-based models ( $0.26\text{--}0.60 \text{ Tg N yr}^{-1}$  (e.g., Li et al., 1996; Del Grosso et al., 2006; Lu et al., 2021).

335 We synthesized a consistent set of field observations representative of long-term means for different croplands across North America and identified a total of 32 observations gathered from 1998 to 2016 (Figs. 4a-b). We summarized the comparison between the model and observations using the normalized mean bias ( $\text{NMB} = \frac{\sum(M_i - O_i)}{\sum O_i}$ , where  $M_i$  and  $O_i$  are modelled and observed) and the squared-correlation coefficient ( $r^2$ ). We found that the model captures well the spatial distribution of soil  $\text{N}_2\text{O}$  in croplands across the U.S.. Simulated soil  $\text{N}_2\text{O}$  fluxes show good agreement with the mean observations over croplands  
340 ( $r^2=0.75$ ) although they are slightly overestimated ( $\text{NMB}=8\%$ ).

We also evaluated the seasonal variability of our simulated soil agriculture  $\text{N}_2\text{O}$  fluxes in the U.S. (Figs. 4c-d) using averaged field observations at the Energy Farm (Blanc-Betes et al., 2020) and regionally averaged monthly fluxes in the Corn Belt from the Carbon Tracker-Lagrange regional inversion framework (Nevison et al., 2018). Figure 4a shows the location of the Energy Farm and the approximate limits of the U.S. Corn Belt. We found that the model represents reasonably well the seasonal  
345 variability of soil  $\text{N}_2\text{O}$  fluxes across the Corn Belt as well as at the Energy Farm in Illinois, with direct agriculture  $\text{N}_2\text{O}$  emissions peaking up early in the growing season (April–May), which coincides with addition of fertilization, as in the observations.

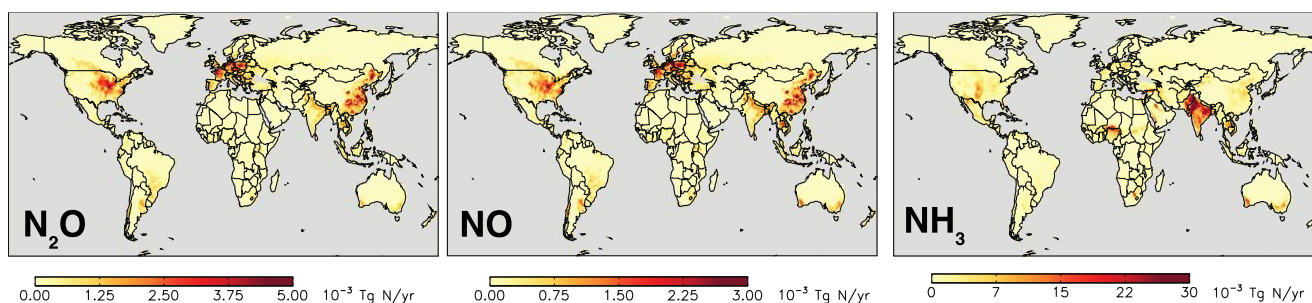
### 3.2 Global soil $\text{NO}$ , $\text{N}_2\text{O}$ and $\text{NH}_3$

We also evaluated soil  $\text{NO}$ ,  $\text{N}_2\text{O}$  and  $\text{NH}_3$  emissions simulated by CLM5 in the global control simulation. Figure 5 presents  
350 the total annual global  $\text{N}_2\text{O}$ ,  $\text{NO}$  and  $\text{NH}_3$  agriculture emissions averaged over 5 years (2010–2014) in our simulations. Soil  $\text{NO}$  and  $\text{NH}_3$  emissions are at above-canopy (sections 2.2.2 and 2.2.3). We also compared our soil gas nitrogen emissions with the available estimates reported in a wide range of global emission inventories (CAM5, CEDS, EDGAR, HEMCO) and previously modeled agriculture fluxes (NMIP, Tian et al., 2018 and Wang et al., 2020) (Table 1).  $\text{NH}_3$  emissions were extensively evaluated in Fung et al., (2020) and we included here a follow-up and briefer validation to assess our small updates  
355 in the parameterization (section 2.3.3).

Emission inventories provide monthly estimates from several agriculture sources, such as synthetic and organic fertilizers, manure management, indirect nitrogen losses, among others and, in some cases, emissions from soils in natural ecosystems. To be able to compare the emissions directly with the CLM5 estimates, we extracted monthly emission estimates and selected the sources to represent as best as possible direct agriculture emissions from synthetic and manure fertilizers. In the case of  
360 HEMCO, which provides soil  $\text{NO}$  emissions from both natural and agricultural soils, we weighted their emissions by the fraction of cropland covering each grid-cell in CLM5. We conducted a spatial comparison of the annual  $\text{N}_2\text{O}$ ,  $\text{NO}$  and  $\text{NH}_3$



emissions from CLM5 and each inventory (grid-cell by grid-cell) by computing the normalized mean bias (NMB) and the Pearson's correlation coefficient ( $r$ ). Table 2 shows the annual totals and a summary of these statistics. Spatial distribution of annual-total  $N_2O$  emission estimated by the inventories and differences with CLM5 are shown in Figs. S5–S7 in SM.



365

**Figure 5: Simulated global soil agriculture  $N_2O$ ,  $NO$  and  $NH_3$  emissions in CLM5 without basalt ('Control Run').**

**Table 2. Summary of agriculture  $N_2O$ ,  $NO$  and  $NH_3$  fluxes. Reported is the total global emission (average  $\pm$  standard deviation of the annual totals), nominal mean bias (NMB) and Pearson's correlation coefficient ( $r$ ).**

Emissions	$N_2O$			$NO$			$NH_3$		
	Total ( $Tg\ N\ yr^{-1}$ )	NMB (%)	$r$	Total ( $Tg\ N\ yr^{-1}$ )	NMB (%)	$r$	Total ( $Tg\ N\ yr^{-1}$ )	NMB (%)	$r$
CLM5	$3.12\pm 0.12$	–	–	$2.17\pm 0.06$	–	–	$15.18\pm 0.39$	–	–
CAMS	–	–	–	$0.72\pm 0.01$	21	0.6	$13.64\pm 0.37$	16	0.5
CEDS	–	–	–	$0.62\pm 0.03$	71	0.5	$14.04\pm 0.51$	11	0.6
EDGAR <sup>a</sup>	1.26	147	0.3	0.41	142	0.5	12.71	22	0.5
HEMCO	–	–	–	$3.53\pm 0.15$	-11	0.4	–	–	–
NMIP	$3.30\pm 1.20^b$	-12	0.4	–	–	–	–	–	–
Wang et al.,	$2.43\pm 0.23$	25	0.4	–	–	–	–	–	–

370 <sup>a</sup>Only monthly data are available for 2010. Reported mean of 2010.

<sup>b</sup>Reported mean  $\pm$  standard deviation of seven models

For  $N_2O$ , CLM5 estimates global direct agriculture emissions of  $3.1\ Tg\ N_2O-N\ yr^{-1}$ , which is in line with previous annual estimates for agriculture sources ( $1.7\text{--}5.8\ Tg\ N\ yr^{-1}$ ; e.g., Del Grosso et al., 2006; Syakila and Kroeze, 2011; Saikawa et al., 2014) and the IPCC 2021 reported values for 2007–2016 ( $3.8\ Tg\ N\ yr^{-1}$ ) (Canadell et al., 2021). Our estimate is higher than the commonly used EDGAR emission inventory ( $1.3\ Tg\ N\ yr^{-1}$ ) and close to modeled estimates ( $2.4\text{--}3.3\ Tg\ N\ yr^{-1}$ ; Tian et al., 2018; Wang et al., 2020). The global  $r$  values are positive, and range between 0.3 and 0.4 across the inventory and models,

375



indicating a fairly good correlation between CLM5 N<sub>2</sub>O emissions and previous global estimates. The global NMB values are small and range between -12 to 25%, showing a good agreement with the reported estimates overall.

380 For global agriculture NO emissions, CLM5 estimates 2.2 Tg NO-N yr<sup>-1</sup>, which is in line with previously reported fertilizer-induced soil NO emissions (0.4–3.5 Tg N yr<sup>-1</sup> e.g., Stehfest and Bouwman, 2006; Crippa et al., 2018; Bennouna et al., 2020; Lin et al., 2021). Our global *r* values lie between 0.4–0.6 across all inventories, indicating a good correlation. Our estimate is higher than three emission inventories (CAM5, CEDS and EDGAR) with a global NMB value between 21 and 147%, but close to the adjusted HEMCO estimate (NMB=-11%).

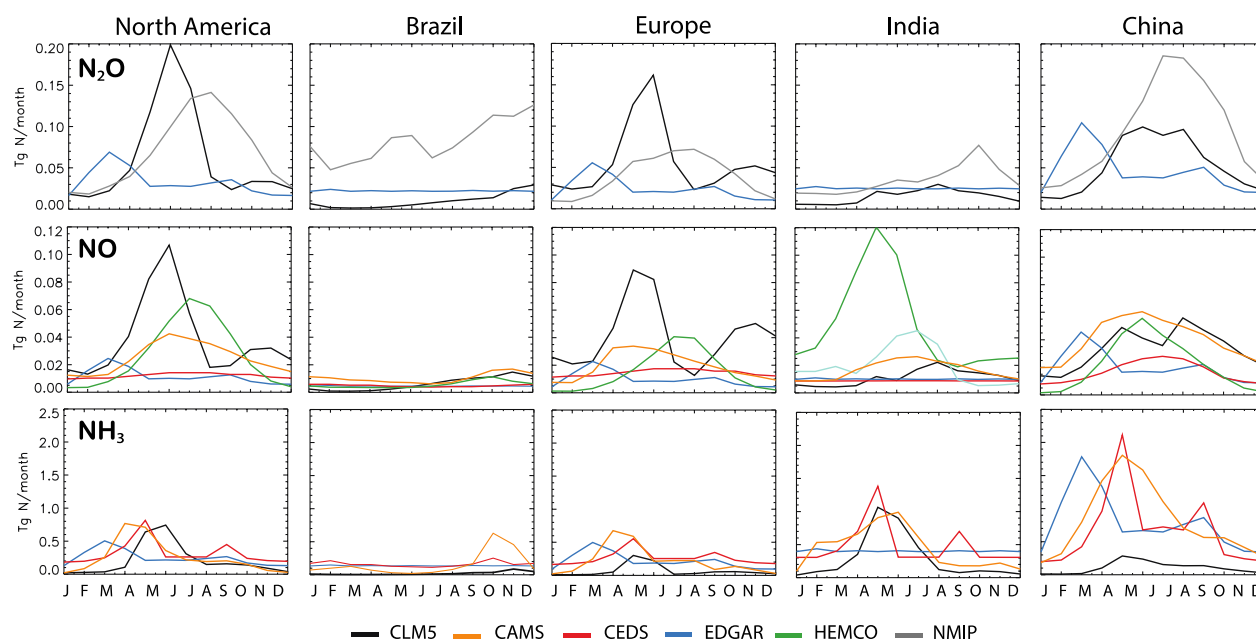
385 Global fertilizer-induced NH<sub>3</sub> emissions in CLM5 are 15.2 Tg NH<sub>3</sub>-N yr<sup>-1</sup>. This estimate is close to estimates (from synthetic and manure fertilizers) reported by Fung et al., (2020) (14 Tg N yr<sup>-1</sup>) and Vira et al., (2020) (18 Tg N yr<sup>-1</sup>) for NH<sub>3</sub> schemes also implemented in CLM5. It is important to note that despite using Fung et al., (2020) NH<sub>3</sub> parameterization in CLM5, our estimate is not exactly as that work because we updated the nitrification and denitrification schemes as well as implemented a dependance on soil pH (section 2.2.3). As indicated by Fung et al., (2020), the CLM5 estimates are slightly higher than three  
390 widely used global emissions inventories (12–14 Tg N yr<sup>-1</sup>; CAM5, CEDS and EDGAR). The global *r* values are 0.5–0.6, indicating a good correlation between CLM5 and all three emission inventories. The high bias in CLM5 is indicated by global NMB values of approximately 11–22% between CLM5 and the emission inventories.

In CLM5 as well as other models and emission inventories, the largest agricultural emissions are found over major cropland regions (Fig. 5 and Figs. S5-S7). However, their spatial distribution differs mostly due to differences in fertilization rates and  
395 application patterns adopted by the models and emission inventories and in some cases, spatial distribution of soil pH. Table 3 summarizes the regional emission totals in our five studied agricultural regions. These areas are major food-producing regions and are responsible for most of the agriculture N<sub>2</sub>O (75%), NO (61%) and NH<sub>3</sub> (55%) emissions with respect to the global total. In CLM5, major crop N<sub>2</sub>O emitters are North America (0.72 Tg N yr<sup>-1</sup>), Europe (0.68 Tg N yr<sup>-1</sup>) and China (0.63 Tg N yr<sup>-1</sup>) each with about 20–23% of global emissions. Soil NO losses are similar, with Europe (0.55 Tg N yr<sup>-1</sup>; 25%), North  
400 America (0.46 Tg N yr<sup>-1</sup>; 21%), and China (0.4 Tg N yr<sup>-1</sup>; 18%) as the largest agriculture sources. As reported by Fung et al (2020), major fertilizer-induced NH<sub>3</sub> emissions in CLM5 are from India (3.48 Tg N yr<sup>-1</sup>; 23%), followed by North America (2.46 Tg N yr<sup>-1</sup>; 16%) and China (1.26 Tg N yr<sup>-1</sup>; 8%).

Figure 6 shows the seasonality of N<sub>2</sub>O, NO and NH<sub>3</sub> emissions in these five main crop regions for CLM5 and global inventories and NMIP. In this analysis, for NMIP N<sub>2</sub>O fluxes we considered the average of only two models as not all seven provided  
405 monthly outputs (Hanqin Tian, Auburn University, personal communication, 2019). In CLM5, each crop has fertilizer applied (as NH<sub>4</sub><sup>+</sup>) evenly over the course of 20 days beginning with leaf emergence (section 2.1). The addition of NH<sub>4</sub><sup>+</sup> in the soil accelerates plant uptake, microbial immobilization, denitrification, nitrification and NH<sub>3</sub> volatilization, which explains why N<sub>2</sub>O, NO and NH<sub>3</sub> emissions peak mostly in spring (March–May) in North America, Europe, China and India and in the fall (October–November) in Brazil. Soil N<sub>2</sub>O and NO fluxes are also strongly dependent on environmental conditions (e.g.,



410 precipitation), which mainly drive the smaller secondary peaks later in the season in North America, Europe and China. All  
global emission inventories and NMIP estimates show similar emission variability, with springtime peaks in the Northern  
hemisphere (North America, Europe, China, and India) and fall peaks in the southern hemisphere (Brazil). For soil  $N_2O$ , the  
seasonality in CLM5 is consistent with that given by the NMIP models although significantly lower in magnitude for Brazil  
and China. However, annual estimates in CLM5 for Brazil ( $0.12 \text{ Tg N yr}^{-1}$ ) and China ( $0.63 \text{ Tg N yr}^{-1}$ ) are in line with the  
415 average from the seven-model ensemble ( $0.20 \text{ Tg N yr}^{-1}$  and  $0.80 \text{ Tg N yr}^{-1}$ , respectively) (Table 3).



420 **Figure 6: Monthly agriculture  $N_2O$ ,  $NO$  and  $NH_3$  emissions in the main crop regions considered in the study (North America, Brazil, Europe, India, and China) estimated by CLM5, CAMS, CEDS, EDGAR, HEMCO and NMIP (Table 1). Soil  $NO$  emissions in HEMCO were weighted by cropland fraction; soil  $N_2O$  in NMIP is the average of only two models that provided monthly output.**

425



**Table 3. Summary of regional agriculture N<sub>2</sub>O, NO and NH<sub>3</sub> fluxes in CLM5 and emission inventories.**

Emissions	North America	Brazil	Europe	India	China
<b>N<sub>2</sub>O (Tg N yr<sup>-1</sup>)</b>					
CLM5	0.72	0.12	0.68	0.18	0.63
EDGAR	0.39	0.27	0.29	0.30	0.55
NMIP	0.30	0.20	0.30	0.50	0.80
<b>NO (Tg N yr<sup>-1</sup>)</b>					
CLM5	0.46	0.10	0.49	0.13	0.40
CAMS	0.17	0.20	0.15	0.24	0.26
CEDS	0.14	0.06	0.18	0.11	0.20
EDGAR	0.14	0.06	0.12	0.12	0.24
HEMCO	0.32	0.07	0.18	0.59	0.27
<b>NH<sub>3</sub> (Tg N yr<sup>-1</sup>)</b>					
CLM5	2.46	0.26	0.82	3.48	1.26
CAMS	3.05	1.88	2.59	5.28	9.71
CEDS	3.75	1.93	3.13	5.66	7.83
EDGAR	2.93	1.64	2.59	4.83	9.33

430 It is important to note that substantial differences among emission inventories exist too. For example, soil N<sub>2</sub>O, NO and NH<sub>3</sub>  
 emissions in EDGAR always peak about one month earlier in the season than the other emission inventories and CLM5; soil  
 NH<sub>3</sub> emissions in CEDS have two seasonal peaks compared to CAMS, CLM5 and EDGAR. As discussed by Fung et al.,  
 (2020), these disparities are primarily caused by differences in the planting season and length of fertilization considered within  
 the inventories as well as the agriculture sources included (e.g., synthetic and/or manure application, manure management,  
 435 etc). In addition, there are systematic uncertainties in the global inventories (e.g., emission factors, environmental conditions,  
 fertilizer types and rates, etc) (Hoesly et al., 2018; Fung et al., 2020). Here we did not intend to understand these differences,  
 rather use the model-inventory comparison to assess the CLM5 performance. We concluded that CLM5 captures well the  
 magnitude and seasonality of direct agriculture nitrogen emissions across the major hotspot regions (North America, Brazil,  
 Europe, India, and China), which are relevant for our study.

440



#### 4 Effect of basalt application on soil nitrogen gas emissions

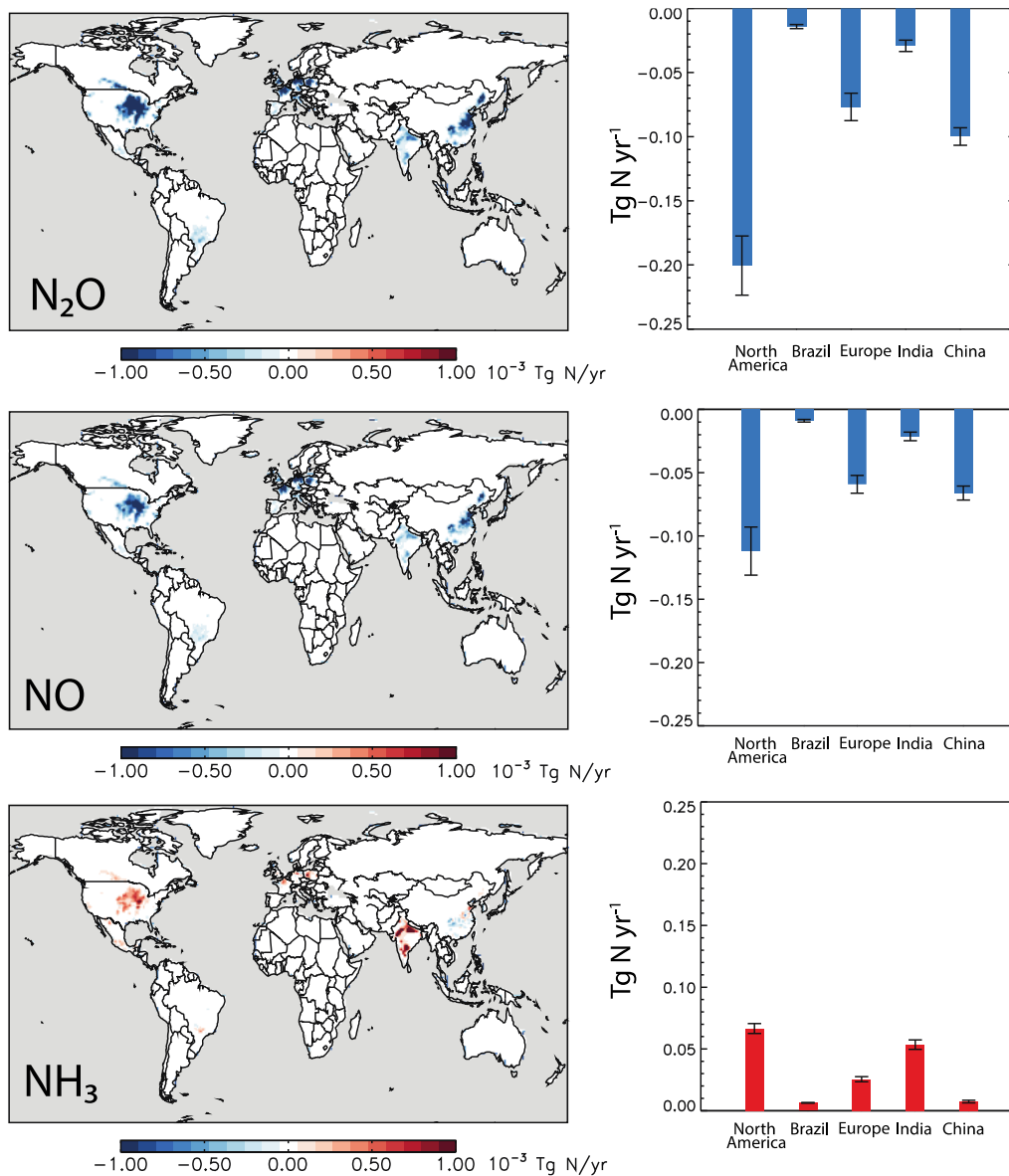
We assessed the regional impact of amending cropland soils with basalt by estimating changes in the nitrogen cycling. We performed this case study by using the soil pH increases after 25 years of repeated annual basalt application as well as optimized deployment locations required to remove 2Gt CO<sub>2</sub> yr<sup>-1</sup> projected by the ERW Model in Beerling et al., (2020) (Figs. 2 and S4). Figure 7 shows the changes in soil N<sub>2</sub>O, NO and NH<sub>3</sub> emissions due to large-scale deployment of ERW with croplands and summarizes the regional changes across the five agricultural regions (North America, Brazil, Europe, India, and China). A close-up view of changes in these five regions are included in Fig. S8 in SM; regional emissions in the Control and ERW runs are summarized in Table 4.

450

**Table 4. Soil N<sub>2</sub>O, NO and NH<sub>3</sub> fluxes in the control and basalt treatment CLM5 runs on main cropland regions. Reported is total emission as average ± standard deviation of the annual totals.**

Region	N <sub>2</sub> O (Tg N yr <sup>-1</sup> )		NO (Tg N yr <sup>-1</sup> )		NH <sub>3</sub> (Tg N yr <sup>-1</sup> )	
	Control	ERW	Control	ERW	Control	ERW
North America	0.72±0.06	0.52±0.04	0.46±0.05	0.35±0.03	2.46±0.33	2.53±0.33
Brazil	0.12±0.01	0.10±0.01	0.10±0.01	0.07±0.01	0.26±0.03	0.27±0.03
Europe	0.68±0.06	0.60±0.05	0.49±0.04	0.43±0.03	0.82±0.05	0.85±0.06
India	0.18±0.02	0.15±0.02	0.13±0.02	0.11±0.01	3.48±0.31	3.53±0.30
China	0.63±0.03	0.53±0.02	0.40±0.02	0.33±0.01	1.26±0.04	1.27±0.04
Total	2.33±0.09	1.90±0.07	1.58±0.07	1.29±0.05	8.28±0.45	8.45±0.46

455



460 **Figure 7: Changes in annual soil N<sub>2</sub>O, NO and NH<sub>3</sub> fluxes across the main five agriculture regions (North America, Brazil, Europe, India, and China) based on increases in soil pH resulting from basalt treatment required to sequester 2 Gt CO<sub>2</sub> yr<sup>-1</sup> (Figure 2). Shown is the spatial distribution of changes in soil N<sub>2</sub>O, NO and NH<sub>3</sub> ( $\Delta$  ERW-Control) and the summary of the regional changes (Tg N yr<sup>-1</sup>). Error bars indicate the standard deviation of the annual total changes.**

Large-scale basalt application consistently decreases soil N<sub>2</sub>O and NO emissions over the five main agriculture regions, with a total decrease of 0.43 Tg N<sub>2</sub>O-N yr<sup>-1</sup> and 0.29 Tg NO-N yr<sup>-1</sup>. These changes are substantial and correspond to 18% of the



total agricultural emissions in those five regions, 8% for N<sub>2</sub>O, and 14% for NO of the global total. Major reductions in N<sub>2</sub>O  
465 and NO occurred in North America (28% for N<sub>2</sub>O and 24% for NO), followed by China (16% and 18%) and Europe (13% and  
12%).

Our new modeling framework only simulates changes in direct soil N<sub>2</sub>O emissions in croplands. Indirect soil nitrogen  
emissions occur through degassing of N<sub>2</sub>O from aquifers and surface waters, via the leaching and runoff of applied N (NO<sub>3</sub>  
and NH<sub>4</sub>) in aquatic systems, and the volatilisation of applied N as NH<sub>3</sub> and NO<sub>x</sub> followed by deposition of NH<sub>4</sub> and NO<sub>x</sub> on  
470 soils and water (Nevison, 2021). ERW field trials in the U.S. have reported nitrogen losses (in the form of NO<sub>3</sub> and NH<sub>4</sub>) to  
leaching in the basalt-treated plots that are substantially larger than the control plots in maize (40%) and miscanthus (17%)  
(Blanc-Betes et al., 2020). However, this indirect contribution to the overall emissions is expected to be small, given that  
indirect emissions account for less than 5% of total agricultural N<sub>2</sub>O emissions (Nevison, 2021; Lu et al., 2022).

Basalt applications increased soil NH<sub>3</sub> emissions as expected, with a total increase of 0.45 Tg NH<sub>3</sub>-N yr<sup>-1</sup>, which is about 2%  
475 of agriculture emissions in our five regions and 1% of the global total. The increasing effect on NH<sub>3</sub> is not as consistent across  
all soils as for N<sub>2</sub>O and NO and some grid cells with acidic soils (pH < 5.5) displayed decreases in NH<sub>3</sub>, especially in regions  
across Brazil and China (Fig. S7). Increases in soil pH favours nitrification and subsequent denitrification processes (Parton  
et al., 1996), which reduces N in the NH<sub>4</sub><sup>+</sup> form in the soils available for NH<sub>3</sub> volatilization. Overall, relatively major increases  
in NH<sub>3</sub> occurred in North America, Brazil and Europe (3–4%), followed by India (1.5%) with marginal increases in China  
480 (0.8%). Regions with more neutral and alkaline soils have more significant increases (8–12%), such as croplands in the U.S.  
with soil pH ranging 6.5–7.5, which showed increases up to 10%.

## 5 Conclusions

We present the development and implementation of new updates and schemes for the CLM5 nitrogen cycle to evaluate the  
potential impact of ERW with croplands. In particular, new updates in N<sub>2</sub>O focus on the gross denitrification and denitrification  
485 end products rates described by Blanc-Betes et al., (2020) based on observations on ERW field trials in the US, and the N<sub>2</sub>O  
nitrification rate. In addition, we implement a new parameterization to calculate NO release from nitrification and  
denitrification processes, considering rain pulses in nitrification and losses of NO to plant canopy. Finally, for NH<sub>3</sub> we use the  
volatilization scheme (Fu et al., 2020), with a regulating pH function based on observations of basalt, lime, and biochar  
applications.

490 Using our global simulations, we successfully validated simulated ‘control’ (i.e., no ERW) seasonal cycles of soil N<sub>2</sub>O, NO  
and NH<sub>3</sub> emissions against a wide range of global emission inventories and previously reported estimates. For N<sub>2</sub>O, we also  
use results from the N<sub>2</sub>O Model Intercomparison Project, the Carbon-Tracker Lagrange North American Regional Inversion  
Framework and a compilation of long-term observations in different croplands across North America. We also benchmarked  
simulated mitigation of soil N<sub>2</sub>O fluxes in response to ERW against a sub-set of data from ERW field trials in the U.S. Corn



495 Belt with single-point simulations at Energy Farm in Illinois (U.S.) and provide a case study of the effect of large-scale ERW  
deployment with croplands on soil nitrogen fluxes across five key regions with high potential for CDR with ERW (North  
America, Brazil, Europe, India, and China).

Our implementations have enabled us to understand the implication of large-scale deployment of ERW with croplands on  
direct soil nitrogen trace gas emissions. Our modelling framework simulates important reductions in both N<sub>2</sub>O and NO (18%)  
500 and moderate increases in NH<sub>3</sub> (2%) across five main cropland regions, using the soil pH increases that would occur after 25-  
year basalt application to remove 2Gt CO<sub>2</sub> per year projected (Beerling et al., 2020). Reductions are most marked over North  
America, with decreases of 28% in N<sub>2</sub>O and 24% in NO and increases of about 10% in NH<sub>3</sub> (for neutral and alkaline agriculture  
soils).

Given agricultural N<sub>2</sub>O emissions account for more than 50% of the total N<sub>2</sub>O emissions (Tian et al., 2020) and these emissions  
505 are expected to continue to grow due to increases in fertilizer usage (IPCC, 2021), regional decreases in N<sub>2</sub>O emissions from  
basalt amendments in croplands are significant and may impact stratospheric ozone. Our study highlights the additional  
potential of ERW for climate change mitigation through reducing emissions of a non-CO<sub>2</sub> greenhouse gas.

Simulated decreases in soil NO emissions and moderate increases in NH<sub>3</sub> from basalt treatments in our five cropland regions  
has further implications for regional air quality. Once emitted from soil, NH<sub>3</sub> undergoes rapid reactions in the atmosphere  
510 forming inorganic NO<sub>3</sub><sup>-</sup> and NH<sub>4</sub><sup>+</sup> aerosols, which contributes to PM<sub>2.5</sub> formation. Agriculture NH<sub>3</sub> emissions are responsible  
for 30% of all PM<sub>2.5</sub> in the U.S., 50% in Europe and 20% in China (e.g., Wyer et al., 2022). Similarly, soil NO is rapidly  
oxidized, generating tropospheric O<sub>3</sub> and secondary organic aerosols (SOA). Ozone is a strong oxidant, which causes harm to  
human health and to crops, and SOA also contributes to PM<sub>2.5</sub>. These past decades, significant government attention has been  
focused on regulating NH<sub>3</sub> emissions as a strategy for reducing PM<sub>2.5</sub> (e.g., U.S. EPA, 2004; UK DEFRA, 2019). However, in  
515 future emission projections, it is unclear whether controlling NH<sub>3</sub> may be an effective strategy for reducing PM<sub>2.5</sub> particularly  
given that NO<sub>x</sub> can also act as the primary limiting precursor for the formation of secondary NH<sub>4</sub><sup>+</sup> aerosols (e.g., Vieno et al.,  
2016). Our study thus provides a scientific modelling tool to aid stakeholders in evaluating global and regional ERW proposals  
as an additional strategy to mitigate climate change and ensuring a clean and sustainable environment.

**Code availability** CLM5.0.25 is publicly available through the Community Terrestrial System Model (CTSM) git repository  
520 (<https://github.com/ESCOMP/ctsm>). Modified CLM5 codes developed are currently being transferred to the new released  
model version (CTSM5.1 dev118) and are available upon request in the meanwhile.

**Data availability** All data used in the study are available from the provided references.

**Author contribution:** MVM developed and implemented the new code, performed the modelling experiments, and analyzed  
the output. EBB, LLT, LKE and WRW provided input for the model development. MVM, EK and DJB designed the modelling  
525 experiment. IBK, MDM, EHD, IC and NJP provided observations collected in ERW field experiments. MVM prepared the  
manuscript with contributions from all co-authors.

**Competing interests:** The authors declare that they have no conflict of interest.



**Acknowledgements:** This work was supported by the UKRI Future Leaders Fellowship Programme awarded to MVM (MR/T019867/1) and the Leverhulme Research Centre Award (RC-2015–02) awarded to DJB. Development of NH<sub>3</sub> emission model was supported in part by the National Natural Science Foundation of China (NSFC)/Research Grants Council (RGC) (grant no. N\_CUHK440/20) awarded by RGC (Hong Kong) to APKT. We thank Cynthia Nevison (INSTAAR), Hanqin Tian (Auburn University), Julius Vira (Finnish Meteorological Institute) and Anthony Wong (University of Boston, now MIT) for helpful discussions. High-performance computing support from Cheyenne (doi:10.5065/D6RX99HX) was provided by NCAR's Computational and Information Systems Laboratory, sponsored by the National Science Foundation under Cooperative Agreement No. 1852977.

## References

- Bakwin, P. S., S. C. Wofsy, S. M. Fan, M. Keller, S. E. Trumbore, and J. M. Da Costa: Emission of nitric oxide from tropical forest soils and exchange of NO between the forest canopy and atmospheric boundary layers, *J. Geophys. Res.*, 95(D10), 16,755–16,764, 1990.
- Blanc-Betes, E, Kantola, IB, Gomez-Casanovas, N, et al.: In silico assessment of the potential of basalt amendments to reduce N<sub>2</sub>O emissions from bioenergy crops. *GCB Bioenergy*, 13: 224–241, <https://doi.org/10.1111/gcbb.12757>, 2020.
- Beerling, D.J., Leake, J.R., Long, S.P., Scholes, J.D., Ton, J., Nelson, P.N., Bird, M.I., Kantzas, E., Taylor, L.L., Sarkar, B., Kelland, M., DeLucia, E., Kantola, I., Müller, C., Rau, G. & Hansen, J.: Farming with crops and rocks to address global climate, food and soil security, *Nature Plants*, 4, 138–147, <https://doi.org/10.1038/s41477-018-0108-y>, 2018.
- Beerling, D.J., Kantzas, E.P., Lomas, M.R. et al.: Potential for large-scale CO<sub>2</sub> removal via enhanced rock weathering with croplands, *Nature*, 583, 242–248, <https://doi.org/10.1038/s41586-020-2448-9>, 2020.
- Beerling, D. J., Epihov, D.Z., Kantola, I.L., Masters, M.D., Reershemius, T., Planavsky, N.J., Reinhard, C.T., Jordan, J., Thorne, S. J., Webber, J., Val Martin, M., Hartley, S.E., Larkin, C., James, R., Pearce, C. DeLucia, E.H. and Banwart, S. A.: Enhanced rock weathering in the U.S. Corn Belt delivers carbon sequestration with agronomic benefits, submitted to *Science*.
- Bennouna, .Y, Christophe, Y., Schulz, M.Y., Christophe, H.J., Eskes, Basart, S., Benedictow, A.-M., Blechschmidt, S, Chabrillat, C.E., Cuevas, H, Flentje, KM, Hansen, UIM, Kapsomenakis, J, Langerock, B, Petersen, K, Richter, A, Sudarchikova, N, Thouret, V, Wagner, A, Wang, Y, Warneke, T, Zerefos, C.: Validation report of the CAMS global Reanalysis of aerosols and reactive gases, years 2003–2019, Copernicus Atmosphere Monitoring Service (CAMS), <http://dx.doi.org/10.24380/2v3p-ab79>, 2020.
- Canadell, J.G., P.M.S. Monteiro, M.H. Costa, L. Cotrim da Cunha, P.M. Cox, A.V. Eliseev, S. Henson, M. Ishii, S. Jaccard, C. Koven, A. Lohila, P.K. Patra, S. Piao, J. Rogelj, S. Syampungani, S. Zaehle, and K. Zickfeld, 2021: Global Carbon and other Biogeochemical Cycles and Feedbacks. In *Climate Change 2021: The Physical Science Basis. Contribution of Working Group I to the Sixth Assessment Report of the Intergovernmental Panel on Climate Change* [Masson-Delmotte, V., P. Zhai, A. Pirani, S.L. Connors, C. Péan, S. Berger, N. Caud, Y. Chen, L. Goldfarb, M.I. Gomis, M. Huang, K. Leitzell, E. Lonnoy,



- 560 J.B.R. Matthews, T.K. Maycock, T. Waterfield, O. Yelekçi, R. Yu, and B. Zhou (eds.]. Cambridge University Press, Cambridge, United Kingdom and New York, NY, USA, pp. 673–816, doi:[10.1017/9781009157896.007](https://doi.org/10.1017/9781009157896.007).
- Chen, Z., Griffis, T. J., Millet, D. B., Wood, J. D., Lee, X., Baker, J. M., Xiao, K., Turner, P. A., Chen, M., Zobitz, J., & Wells, K. C. : Partitioning N<sub>2</sub>O emissions within the U.S. Corn Belt using an inverse modeling approach, *Global Biogeochemical Cycles*, 30(8), 1192–1205, <https://doi.org/10.1002/2015G B005313>, 2016.
- 565 Cheng, Y., Huang, M., Chen, M., Guan, K., Bernacchi, C., Peng, B., and Tan, Z.: Parameterizing perennial bioenergy crops in Version 5 of the Community Land Model based on site-level observations in the Central Midwestern United States, *Journal of Advances in Modelling Earth Systems*, 12, e2019MS001719. <https://doi.org/10.1029/2019MS001719>, 2020.
- Chiaravalloti, I. Observed ammonia fluxes during maize production in mesocosms with basalt amendments. *ESS Open Archive*, February 27, 2023, DOI: 10.22541/essoar.167751584.47065180/v1.
- 570 Crippa, M., Guizzardi, D., Muntean, M., Schaaf, E., Dentener, F., Van Aardenne, J. A., Monni, S., Doering, U., Olivier, J. G. J., Pagliari, V., and Janssens-Maenhout, G.: Gridded emissions of air pollutants for the period 1970–2012 within EDGAR v4.3.2, 10, 1987–2013, <https://doi.org/10.5194/essd-10-1987-2018>, 2018.
- Danabasoglu, G., Lamarque, J.-F., Bacmeister, J., Bailey, D. A., DuVivier, A. K., Edwards, J., et al.: The Community Earth System Model Version 2 (CESM2). *Journal of Advances in Modeling Earth Systems*, 12, e2019MS001916. <https://doi.org/10.1029/2019MS001916>, 2020.
- 575 Davidson, E. A. and Trumbore, S. E.: Gas diffusivity and production of CO<sub>2</sub> in deep soils of the eastern Amazon, *Tellus B*, 47, 550–565, <https://doi.org/10.1034/j.1600-0889.47.issue5.3.x>, 1995
- Davidson, E.A. and Verchot, L.V.: Testing the hole-in-the-pipe model of nitric and nitrous oxide emissions from soils using the TRAGNET data base, *Global Biogeochem. Cycles*, 14, 1035–1043, 2000.
- 580 Davidson, E. A. and Kanter, D.: Inventories and scenarios of nitrous oxide emissions, *Environ. Res. Lett.* 9, 105012, 2014.
- Del Grosso, S. J., Parton, W. J., Mosier, A. R., Ojima, D. S., Kulmala, A. E., & Phongpan, S.: General model for N<sub>2</sub>O and N<sub>2</sub> gas emissions from soils due to denitrification, *Global Biogeochemical Cycles*, 14, 1045–1060, <https://doi.org/10.1029/1999G B001225>, 2000.
- Del Grosso, S. J., Parton, W. J., Mosier, A. R., Walsh, M. K., Ojima, D. S., & Thornton, P. E.: DAYCENT national-scale simulations of nitrous oxide emissions from cropped soils in the United States. *Journal of Environmental Quality*, 35, 1451–1460. <https://doi.org/10.2134/jeq2005.0160>, 2006.
- 585 Drewniak, B., Song, J., Prell, J., Kotamarthi, V. R., and Jacob, R.: Modeling agriculture in the Community Land Model, *Geosci. Model Dev.*, 6, 495–515, <https://doi.org/10.5194/gmd-6-495-2013>, 2013.



- Food and Agriculture organization (FAO) of the United Nations, Harmonized World Soil Database (version 1.2). Food  
590 Agriculture Organization, Rome, Italy and IIASA, Laxenburg, Austria, 2012.  
(<http://webarchive.iiasa.ac.at/Research/LUC/External-World-soil-database/HTML/>)
- Firestone, M.K. and Davidson, E.A.: Microbiological Basis of NO and N<sub>2</sub>O Production and Consumption in Soils. In:  
Andreae, M.O. and Schimel, D.S., Eds., Exchange of Trace Gases between Terrestrial Ecosystems and the Atmosphere, John  
Wiley and Sons, New York, 7-21, 1989.
- 595 Fung, K. M., Val Martin, M., and Tai, A. P. K.: Modeling the interinfluence of fertilizer-induced NH<sub>3</sub> emission, nitrogen  
deposition, and aerosol radiative effects using modified CESM2, Biogeosciences, 19, 1635–1655, <https://doi.org/10.5194/bg-19-1635-2022>, 2022.
- Fuss, S., Canadell, J., Peters, G. et al.: Betting on negative emissions, Nature Clim Change, 4, 850–853,  
<https://doi.org/10.1038/nclimate2392>, 2014.
- 600 Griffis, T. J., Lee, X., Baker, J. M., Russelle, M. P., Zhang, X., Venterea, R., & Millet, D. B.: Reconciling the differences  
between top-down and bottom-up estimates of nitrous oxide emissions for the U.S. Corn Belt. Global Biogeochemical Cycles,  
27(3), 746–754, <https://doi.org/10.1002/gbc.20066>, 2013.
- Hoesly, R. M., Smith, S. J., Feng, L., Klimont, Z., Janssens-Maenhout, G., Pitkanen, T., Seibert, J. J., Vu, L., Andres, R. J.,  
Bolt, R. M., Bond, T. C., Dawidowski, L., Kholod, N., Kurokawa, J., Li, M., Liu, L., Lu, Z., Moura, M. C. P., ORourke, P. R.,  
605 and Zhang, Q.: Historical (1750–2014) anthropogenic emissions of reactive gases and aerosols from the Community Emissions  
Data System (CEDS), 11, 369–408, <https://doi.org/10.5194/gmd-11-825-369-2018>, 2018.
- Hudman, R. C., Moore, N. E., Mebust, A. K., Martin, R. V., Russell, A. R., Valin, L. C., and Cohen, R. C.: Steps towards a  
mechanistic model of global soil nitric oxide emissions: implementation and space based-constraints, Atmos. Chem. Phys.,  
12, 7779–7795, <https://doi.org/10.5194/acp-12-7779-2012>, 2012.
- 610 Hurtt, G. C., Chini, L. P., Frohking, S., Betts, R. A., Feddema, J., Fischer, G., Fisk, J. P., Hibbard, K., Houghton, R. A., Janetos,  
A., Jones, C. D., Kindermann, G., Kinoshita, T., Klein Goldewijk, K., Riahi, K., Shevliakova, E., Smith, S., Stehfest, E.,  
Thomson, A., Thornton, P., van Vuuren, D. P., and Wang, Y. P.: Harmonization of land-use scenarios for the period 1500–  
2100: 600 years of global gridded annual land-use transitions, wood harvest, and resulting secondary lands, Clim. Change,  
109, 117–161, <https://doi.org/10.1007/s10584-011-0153-2>, 2011.
- 615 Inatomi M, Hajima T, Ito A. : Fraction of nitrous oxide production in nitrification and its effect on total soil emission: A meta-  
analysis and global-scale sensitivity analysis using a process-based model. PLoS ONE 14(7): e0219159.  
<https://doi.org/10.1371/journal.pone.0219159>, 2019.
- IPCC, 2021: *Climate Change 2021: The Physical Science Basis. Contribution of Working Group I to the Sixth Assessment  
Report of the Intergovernmental Panel on Climate Change*[Masson-Delmotte, V., P. Zhai, A. Pirani, S.L. Connors, C. Péan,



- 620 S. Berger, N. Caud, Y. Chen, L. Goldfarb, M.I. Gomis, M. Huang, K. Leitzell, E. Lonnoy, J.B.R. Matthews, T.K. Maycock, T. Waterfield, O. Yelekçi, R. Yu, and B. Zhou (eds.]. Cambridge University Press, Cambridge, United Kingdom and New York, NY, USA, In press, doi:10.1017/9781009157896.
- Jacob, D. J., and S. C. Wofsy : Budgets of reactive nitrogen, hydrocarbons and ozone over the Amazon forest during the wet season, *J. Geophys. Res.*, 95(D10), 16,737– 16,754, 1990.
- 625 Johansson, C., Rodhe, H. and Sanhuenza, E. : Emission of NO in a tropical savanna and a cloud forest during the dry season, *J. Geophys. Res.*, 93(D6), 7180–7192, 1988.
- Kantzas, E.P., Val Martin, M., Lomas, M.R. et al.: Substantial carbon drawdown potential from enhanced rock weathering in the United Kingdom, *Nat. Geosci.* 15, 382–389, <https://doi.org/10.1038/s41561-022-00925-2>, 2022.
- Kim, M.-S.; Min, H.-G.; Koo, N.; Kim, J.-G: Response to Ammonia Emission Flux to different pH Conditions under Biochar and Liquid Fertilizer Application, *Agriculture*, 11, 136. <https://doi.org/10.3390/agriculture11020136>, 2022.
- 630 Kantola, I. B., Masters, M.D., Beerling, D. J., Long, S. P., and DeLucia, E .H.: Potential of global croplands and bioenergy crops for climate change mitigation through deployment for enhanced weathering. *Biol. Lett.* 13, 20160714, <https://doi.org/10.1098/rsbl.2016.0714>, 2017.
- Koven, C. D., Riley, W. J., Subin, Z. M., Tang, J. Y., Torn, M. S., Collins, W. D., Bonan, G. B., Lawrence, D. M., and Swenson, S. C.: The effect of vertically resolved soil biogeochemistry and alternate soil C and N models on C dynamics of CLM4, *Biogeosciences*, 10, 7109–7131, <https://doi.org/10.5194/bg-10-7109-2013>, 2013.
- 635 Lawrence, D., Fisher, R., Koven, C., Swenson, S., and Vertenstein, M.: Technical Description of version 5.0 of the Community Land Model (CLM), [http://www.cesm.ucar.edu/models/cesm2/land/CLM50\\_Tech\\_Note.pdf](http://www.cesm.ucar.edu/models/cesm2/land/CLM50_Tech_Note.pdf), last access: January 12, 2023.
- Lawrence, D. M., Fisher, R. A., Koven, C. D., Oleson, K. W., Swenson, S. C., Bonan, G., Collier, N., Ghimire, B., Kampenhout, L., Kennedy, D., Kluzek, E., Lawrence, P. J., Li, F., Li, H., Lombardozzi, D., Riley, W. J., Sacks, W. J., Shi, M., Vertenstein, M., Wieder, W. R., Xu, C., Ali, A. A., Badger, A.M., Bisht, G., Broeke, M., Brunke, M. A., Burns, S. P., Buzan, J., Clark, M., Craig, A., Dahlin, K., Drewniak, B., Fisher, J.B., Flanner, M., Fox, A. M., Gentine, P., Hoffman, F., Keppel-Aleks, G., Knox, R., Kumar, S., Lenaerts, J., Leung, L. R., Lipscomb, W. H., Lu, Y., Pandey, A., Pelletier, J. D., Perket, J., Randerson, J. T., Ricciuto, D. M., Sanderson, B. M., Slater, A., Subin, Z. M., Tang, J., Thomas, R. Q., Val Martin, M., and Zeng, X.: The Community Land Model Version 5: Description of New Features, Benchmarking, and Impact of Forcing Uncertainty, *J. Adv. Model. Earth Syst.*, 11, 4245–4287, <https://doi.org/10.1029/2018MS001583>, 2019.
- 645 Lawrence, P. J. and Chase, T. N.: Representing a new MODIS consistent land surface in the Community Land Model (CLM 3.0), *J. Geophys. Res.*, 112, G01023, <https://doi.org/10.1029/2006JG000168>, 2007.



- Levis, S., Badger, A., Drewniak, B., Nevison, C., and Ren, X.: CLM crop yields and water requirements: avoided impacts by  
650 choosing RCP 4.5 over 8.5, *Clim. Change*, 146, 501–515, <https://doi.org/10.1007/s10584-016-1654-9>, 2018.
- Li, C., Narayanan, V., & Harriss, R. C.: Model estimates of nitrous oxide emissions from agricultural lands in the United States. *Global Biogeochemical Cycles*, 10(2), 297–306. <https://doi.org/10.1029/96GB00470>, 1996.
- Li, C., Aber, J., Stange, F., Butterbach-Bahl, K. and Papen, H.: A process-oriented model of N<sub>2</sub>O and NO emissions from forest soils: 1. Model development. *J. Geophys. Res.* 105(D4):4369-4384, 2000.
- 655 Li, C., Salas, W., Zhang, R., Krauter, C., Rotz, A., and Mitloehner, F.: Manure-DNDC: a biogeochemical process model for quantifying greenhouse gas and ammonia emissions from livestock manure systems, *Nutr. Cycl. Agroecosyst.*, 93, 163–200, <https://doi.org/10.1007/s10705-012-9507-z>, 2012.
- Lin, H., Jacob, D. J., Lundgren, E. W., Sulprizio, M. P., Keller, C. A., Fritz, T. M., Eastham, S. D., Emmons, L. K., Campbell, P. C., Baker, B., Saylor, R. D., and Montuoro, R.: Harmonized Emissions Component (HEMCO) 3.0 as a versatile emissions  
660 component for atmospheric models: application in the GEOS-Chem, NASA GEOS, WRF-GC, CESM2, NOAA GEFS-Aerosol, and NOAA UFS models, *Geosci. Model Dev.*, 14, 5487–5506, <https://doi.org/10.5194/gmd-14-5487-2021>, 2021.
- Liu, B., M. rkved, P. T., Frosteg. rd, ..., & Bakken, L. R.: Denitrification gene pools, transcription and kinetics of NO, N<sub>2</sub>O and N<sub>2</sub> production as affected by soil pH. *FEMS Microbiology Ecology*, 72, 407–417, <https://doi.org/10.1111/j.1574-6941.2010.00856.x>, 2010.
- 665 Lombardozzi, D. L., Lu, Y., Lawrence, P. J., Lawrence, D. M., Swenson, S., Oleson, K. W., Wieder, W. R., and Ainsworth, E. A.: Simulating Agriculture in the Community Land Model Version 5, *J. Geophys. Res.-Biogeo.*, 125, e2019JG005529, <https://doi.org/10.1029/2019JG005529>, 2020
- Lu, C., Yu, Z., Zhang, J., Cao, P., Tian, H., & Nevison, C.: Century-long changes and drivers of soil nitrous oxide (N<sub>2</sub>O) emissions across the contiguous United States. *Global Change Biology*, 28, 2505– 2524, <https://doi.org/10.1111/gcb.16061>,  
670 2022.
- Martin, R. E., M. C. Scholes, A. R. Mosier, D. S. Ojima, E. A. Holland, and W. J. Parton: Controls on annual emissions of nitric oxide from soils of the Colorado shortgrass steppe, *Global Biogeochem. Cycles*, 12(1), 81–91, 1998.
- Miller, S. M., Kort, E. A., Hirsch, A. I., Dlugokencky, E. J., Andrews, A. E., Xu, X., Tian, H., Nehrkorn, T., Eluszkiewicz, J., Michalak, A. M. and Wofsy, S. C.: Regional sources of nitrous oxide over the United States: Seasonal variation and spatial  
675 distribution, *Journal of Geophysical Research Atmospheres*, 117(6), D06310. <https://doi.org/10.1029/2011JD016951>, 2012.
- Mkhabela, M.S., Gordon, R., Burton, D. et al.: Effect of lime, dicyandiamide and soil water content on ammonia and nitrous oxide emissions following application of liquid hog manure to a marshland soil. *Plant Soil*, 284, 351–361. <https://doi.org/10.1007/s11104-006-0056-6>, 2006.



- 680 National Research Council, Climate Intervention: Carbon Dioxide Removal and Reliable Sequestration. *Washington, DC: The National Academies Press*. <https://doi.org/10.17226/18805>, 2015.
- Nevison, C., Andrews, A., Thoning, K., Dlugokencky, E., Sweeney, C., Miller, S., Saikawa, E., Benmergui, J., Fischer, M., Mountain, M., & Nehrkorn, T. : Nitrous oxide emissions estimated with the carbontracker-Lagrange North American regional inversion framework, *Global Biogeochemical Cycles*, 32(3), 463–485. <https://doi.org/10.1002/2017GB005759>, 2018.
- Nevison, C., IPCC Good Practice Guidance and Uncertainty Management in National Greenhouse Gas Inventories, Indirect  
685 N<sub>2</sub>O emissions from nitrogen used in agriculture, [https://www.ipcc-nggip.iges.or.jp/public/gp/english/4\\_Agriculture.pdf](https://www.ipcc-nggip.iges.or.jp/public/gp/english/4_Agriculture.pdf), 2021, Last accessed February 9, 2023.
- Nevison, C., Goodale, C., Hess, P., Wieder, W. R., Vira, J. and Groffman, P.M.: Nitrification and Denitrification in the Community Land Model Compared with Observations at Hubbard Brook Forest, *Ecological Applications* e2530. <https://doi.org/10.1002/eap.2530>, 2022a.
- 690 Nevison, C., Hess, P., Goodale, C., Zhu, Q. and Vira, J.: Nitrification, Denitrification, and Competition for Soil N: Evaluation of Two Earth System Models against Observations, *Ecological Applications* e252, <https://doi.org/10.1002/eap.2528>, 2022b.
- Parton, W. J., Mosier, A. R., Ojima, D. S., Valentine, D. W., Schimel, D. S., Weier, K., & Kulmala, A. E.: Generalized model for N<sub>2</sub> and N<sub>2</sub>O production from nitrification and denitrification. *Global Biogeochemical Cycles*, 10, 401–412. <https://doi.org/10.1029/96GB01455>, 1996.
- 695 Parton, W. J., Holland, E. A., Del Grosso, S. J., Hartman, M. D., Martin, R. E., Mosier, A. R., Ojima, D. S., & Schimel, D. S.: Generalized model for NO<sub>x</sub> and N<sub>2</sub>O emissions from soils. *Journal of Geophysical Research: Atmospheres*, 106, 17403–17419. <https://doi.org/10.1029/2001JD900101>, 2001.
- Portmann, F. T., Siebert, S., and Döll, P.: MIRCA2000-Global monthly irrigated and rainfed crop areas around the year 2000: A new high-resolution data set for agricultural and hydrological modelling: MONTHLY IRRIGATED AND RAINFED CROP  
700 AREAS, *Global Biogeochem. Cy.*, 24, GB1011, <https://doi.org/10.1029/2008GB003435>, 2010.
- Prather, M. J. et al.: Measuring and modelling the lifetime of nitrous oxide including its variability, *J. Geophys. Res. D* 120, 5693–5705, 2015.
- Reay, D. S. et al.: Global agriculture and nitrous oxide emissions, *Nat. Clim. Change* 2, 410–416, 2012.
- Royal Society and Royal Academy of Engineering, Greenhouse gas removal ISBN: 978-1-78252-349-9,  
705 <https://royalsociety.org/topics-policy/projects/greenhouse-gas-removal/> (Last accessed 31 January, 2023), 2018.
- Rochester, I. J.: Estimating nitrous oxide emissions from flood-irrigated alkaline grey clays, *Soil Research*, 41, 197–206. <https://doi.org/10.1071/sr02068>, 2003.



Saikawa, E., Prinn, R. G., Dlugokencky, E., Ishijima, K., Dutton, G. S., Hall, B. D., Langenfelds, R., Tohjima, Y., Machida, T., Manizza, M., Rigby, M., O'Doherty, S., Patra, P. K., Harth, C. M., Weiss, R. F., Krummel, P. B., van der Schoot, M.,  
710 Fraser, P. J., Steele, L. P., Aoki, S., Nakazawa, T., and Elkins, J. W.: Global and regional emissions estimates for N<sub>2</sub>O, Atmos. Chem. Phys., 14, 4617–4641, <https://doi.org/10.5194/acp-14-4617-2014>, 2014.

Sha Z., Qianqian Li, Tiantian Lv, Tom Misselbrook, Xuejun Liu: Response of ammonia volatilization to biochar addition: A meta-analysis, Science of The Total Environment, 655, 1387-1396, ISSN 0048-9697, [https://doi.org/10.1016/j.scitotenv.2018.11.316\\_2019](https://doi.org/10.1016/j.scitotenv.2018.11.316_2019).

715 Shcherbak I., Millar, N., and Robertson, G.P.: Global metaanalysis of the nonlinear response of soil nitrous oxide (N<sub>2</sub>O) emissions to fertilizer nitrogen, PNAS 111, 9199-9204, 2014.

Stehfest, E. and Bouwman, L.: N<sub>2</sub>O and NO Emission from Agricultural Fields and Soils under Natural Vegetation: Summarizing Available Measurement Data and Modeling of Global Annual Emissions. Nutrient Cycling in Agroecosystems, 74, 207-228. 597 <http://dx.doi.org/10.1007/s10705-006-9000-7>, 2006.

720 Syakila, A., & Kroeze, C.: The global nitrous oxide budget revisited. Greenhouse Gas Measurement and Management, 1(1), 17–26., <https://doi.org/10.3763/ghgmm.2010.0007>, 2011.

Sutton, M. A., Reis, S., Riddick, S. N., Dragosits, U., Nemitz, E., Theobald, M. R., Tang, Y. S., Braban, C. F., Vieno, M., Dore, A. J., Mitchell, R. F., Wanless, S., Daunt, F., Fowler, D., Blackall, T. D., Milford, C., Flechard, C. R., Loubet, B., Massad, R., Cellier, P., Personne, E., Coheur, P. F., Clarisse, L., Van Damme, M., Ngadi, Y., Clerbaux, C., Skjøth, C. A.,  
725 Geels, C., Hertel, O., Wichink Kruit, R. J., Pinder, R. W., Bash, J. O., Walker, J. T., Simpson, D., Horváth, L., Misselbrook, T. H., Bleeker, A., Dentener, F., and de Vries, W.: Towards a climate-dependent paradigm of ammonia emission and deposition, Philos. T. Roy. Soc. B, 368, 20130166, <https://doi.org/10.1098/rstb.2013.0166>, 2013.

Tian, H., Yang, J., Lu, C., Xu, R., Canadell, J. G., Jackson, R. B., Arneth, A., Chang, J., Chen, G., Ciais, P., Gerber, S., Ito, A., Huang, Y., Joos, F., Lienert, S., Messina, P., Olin, S., Pan, S., Peng, C., Zhu, Q.: The global N<sub>2</sub>O model intercomparison project, Bulletin of the American Meteorological Society, 99(6), 1231–1251. <https://doi.org/10.1175/BAMS-D-17-0212.1>,  
730 2018.

Tian, H., Yang, J., Xu, R., Lu, C., Canadell, J. G., Davidson, E. A., Jackson, R. B., Arneth, A., Chang, J., Ciais, P., Gerber, S., Ito, A., Joos, F., Lienert, S., Messina, P., Olin, S., Pan, S., Peng, C., Saikawa, E., Zhang, B.: Global soil nitrous oxide emissions since the preindustrial era estimated by an ensemble of terrestrial biosphere models: Magnitude, attribution, and uncertainty.  
735 Global Change Biology, 25(2), 640–659. <https://doi.org/10.1111/gcb.14514>, 2019.

U.K. Department for Environment, Food and Rural Affairs (DEFRA), Clean Air Strategy 2019, <https://www.gov.uk/government/publications/clean-air-strategy-2019>, last access: 25 January 2023.



- U.S. Environmental Protection Agency (EPA), The Particle Pollution Report: Current Understanding of Air Quality and Emissions through 2003; EPA 454-R-04-002; U.S. Government Printing Office: Washington, DC, 2004.
- 740 U.S. Environmental Protection Agency (EPA): Inventory of U.S. Greenhouse Gas Emissions and Sinks: 1990-2020. U.S. Environmental Protection Agency, EPA 430-R-22-003, <https://www.epa.gov/ghgemissions/draft-inventory-us-greenhouse-gas-emissions-and-sinks-1990-2020>, 2022.
- Van Damme, M., Clarisse, L., Franco, B., Sutton, M.A., Willem Erisman, J., Wichink Kruit, R., van Zanten, M., Whitburn, S., Hadji-Lazaro, J., Hurtmans, D., Clerbaux, C., Coheur, P.-F: Global, regional, and national trends of atmospheric ammonia derived from a decadal (2008-2018) satellite record, *Environ. Res. Lett.* 16 <https://doi.org/10.1088/1748-9326/abd5e0>, 2021.
- 745 Vieno, M., Heal, M. R., Williams, M. L., Carnell, E. J., Nemitz, E., Stedman, J. R., and Reis, S.: The sensitivities of emissions reductions for the mitigation of UK PM<sub>2.5</sub>, *Atmos. Chem. Phys.*, 16, 265–276, <https://doi.org/10.5194/acp-16-265-2016>, 2016.
- Vira, J., Hess, P., Melkonian, J., and Wieder, W. R.: An improved mechanistic model for ammonia volatilization in Earth system models: Flow of Agricultural Nitrogen version 2 (FANv2), *Geosci. Model Dev.*, 13, 4459–4490, <https://doi.org/10.5194/gmd-13-4459-2020>, 2020.
- 750 Wagena, M. B., Bock, E. M., Sommerlot, A. R., Fuka, D. R., & Easton, Z. M.: Development of a nitrous oxide routine for the SWAT model to assess greenhouse gas emissions from agroecosystems. *Environmental Modelling and Software*, 89, 131–143. <https://doi.org/10.1016/j.envsoft.2016.11.013>, 2017.
- Wang, Q., Feng Zhou, Ziyin Shang, Philippe Ciais, Wilfried Winiwarter, Robert B Jackson, Francesco N Tubiello, Greet  
755 Janssens-Maenhout, Hanqin Tian, Xiaoqing Cui, Josep G Canadell, Shilong Piao, Shu Tao: Data-driven estimates of global nitrous oxide emissions from croplands, *National Science Review*, 7, 2, 441–452, <https://doi.org/10.1093/nsr/nwz087>, 2020.
- Wang, Y., Guo, J., Vogt, R.D., Mulder, J., Wang, J., and Zhang, X: Soil pH as the chief modifier for regional nitrous oxide emissions: New evidence and implications for global estimates and mitigation, *Global Change Biology* 24, 617–626, 2018.
- Wieder, W.R., J. Boehnert, G.B. Bonan, and M. Langseth: RegridDED Harmonized World Soil Database v1.2. Data set.  
760 Available on-line [<http://daac.ornl.gov>] from Oak Ridge National Laboratory Distributed Active Archive Center, Oak Ridge, Tennessee, USA, <http://dx.doi.org/10.3334/ORNLDAAAC/1247>, 2014.
- Wyer, K. E., Kelleghan, D. B., Blanes-Vidal, V., Schaubberger, G., Curran, T. P.: Ammonia emissions from agriculture and their contribution to fine particulate matter: A review of implications for human health, *Journal of Environmental Management*, Volume 323, 116285, ISSN 0301-4797, <https://doi.org/10.1016/j.jenvman.2022.116285>, 2022.
- 765 Xia, Y., Mitchell, K., Ek, M., Sheffield, J., Cosgrove, B., Wood, E., et al.: Continental-scale water and energy flux analysis and validation for the North American Land Data Assimilation System project phase 2 (NLDAS-2): 1. Intercomparison and application of model products. *Journal of Geophysical Research*, 117, D03109, <https://doi.org/10.1029/2011JD016048>, 2012.



Yan, X., Ohara, T., and Akimoto, H.: Statistical modelling of global soil NO<sub>x</sub> emissions, *Global Biogeochem. Cy.*, 19, GB3019, doi:10.1029/2004GB002276, 2005.

770 Yienger, J. J. and Levy II, H.: Empirical model of global soil biogenic NO<sub>x</sub> emissions, *J. Geophys. Res.*, 100, 11447–11464, 1995.

Yoneyama, T., Hashimoto, A. and Totsuka, T.: Absorption of atmospheric NO<sub>2</sub> by plants and soils, *Soil Science and Plant Nutrition*, 26:1, 1-7, DOI: 10.1080/00380768.1980.10433207, 1980.

775 Zeri, M., Anderson-Teixeira, K., Hickman, G., Masters, M., DeLucia, E., & Bernacchi, C. J.: Carbon exchange by establishing biofuel crops in Central Illinois. *Agriculture, Ecosystems and Environment*, 144(1), 319–329. <https://doi.org/10.1016/j.agee.2011.09.006>, 2011.

Zhao, Y., Zhang, L., Tai, A. P. K., Chen, Y., and Pan, Y.: Responses of surface ozone air quality to anthropogenic nitrogen deposition in the Northern Hemisphere, 17, 9781–9796, <https://doi.org/10.5194/acp-17-9781-2017>, 2017.

780